ANGPTL4 from adipose, but not liver, is responsible for regulating plasma triglyceride partitioning

Kathryn M. Spitler[1], Shwetha K. Shetty[1], Emily M. Cushing[1], Kelli L. Sylvers-Davie[1], and Brandon S.J. Davies[1]*

[1] Department of Biochemistry, Fraternal Order of Eagles Diabetes Research Center, and Obesity Research and Education Initiative, University of Iowa, Iowa City, IA 52242

Running Title: Tissue specific loss of Angptl4

*Address Correspondence to: Brandon S. J. Davies, Department of Biochemistry, University of Iowa, 169 Newton Rd., PBDB 3326, Iowa City, IA, 52242. Tel.: 319-335-3225; Fax: 319-335-9570; E-mail: Brandon-davies@uiowa.edu.

Keywords: triglyceride, lipase, lipolysis, lipoprotein metabolism, obesity, glucose homeostasis, adipose

ABSTRACT

Elevated plasma triglyceride levels are associated with metabolic disease. Angiopoietin-like protein 4 (ANGPTL4) regulates plasma triglyceride levels by inhibiting lipoprotein lipase (LPL). ANGPTL4-deficient mice have decreased plasma triglyceride levels and increased adipose triglyceride uptake. ANGPTL4 is largely expressed by adipose and liver; therefore, we generated adipose- and liver-specific ANGPTL4 knockout mice. Mice lacking adipose ANGPTL4 recapitulated the triglyceride phenotypes of whole-body ANGPTL4 deficiency, whereas mice lacking liver ANGPTL4 had no triglyceride phenotypes. When fed a high fat diet (HFD) mice deficient in adipose ANGPTL4 gained more weight, had enhanced adipose LPL activity, and initially had improved glucose and insulin sensitivity. However, this improvement was largely lost after 6 months on HFD. Conversely, liver-deficient ANGPTL4 mice initially displayed no differences in glucose homeostasis, but began to manifest improved glucose tolerance after 6 months on HFD. We conclude that adipose derived ANGPTL4 is responsible for triglyceride regulation, while both adipose- and liver-derived ANGPTL4 may play a role in glucose homeostasis.

INTRODUCTION

Elevated plasma triglyceride levels have been implicated in the pathology of a variety of cardiovascular and metabolic diseases. Circulating triglycerides are hydrolyzed by lipoprotein lipase (LPL), releasing fatty acids that are taken up and utilized by tissues. Angiopoietin-like protein 4 (ANGPTL4), a secreted factor induced by fasting and expressed highly in adipose and liver, inhibits LPL activity and thereby regulates plasma triglyceride levels (1–4). Genetic loss of ANGPTL4 leads to decreased fasting plasma triglyceride levels in both humans and mice, and humans deficient in ANGPTL4 appear to be protected from cardiovascular disease (5–7). Moreover, a recent study found that human carriers of the common inactivating mutant E40K were protected against obesity-associated dyslipidemia (8). However, whether these protections are conferred by loss of ANGPTL4 in a specific tissue or require systemic loss of ANGPTL4 remains unclear.

We have previously shown that *Angptl4* mRNA expression is rapidly induced within 2 hours of fasting (9). We also found that fasted *Angptl4*$^{-/-}$ mice have increased uptake of triglycerides specifically into adipose tissues together with enhanced adipose LPL activity. We developed a model where, during fasting, adipose-derived ANGPTL4 acts locally to inhibit adipose LPL activity and triglyceride uptake (9). This conclusion was further supported by a recent study showing similar phenotypes in adipose-specific *Angptl4* knockout mice (10). ANGPTL4 is also expressed in other metabolically active tissues, especially the liver. The role of ANGPTL4 in the liver remains unclear. Furthermore, the role of ANGPTL4 in mediating or alleviating metabolic disturbances induced by high-fat feeding has not been fully studied. Such studies have been hindered by the fact that *Angptl4*$^{-/-}$ mice fed a high fat diet (HFD) develop a lethal intestinal injury and lymphatic nodule inflammation (11).

In this study, we sought to define the tissue-specific actions of ANGPTL4 more clearly. To this end, we generated adipose and liver-specific *Angptl4* knockout mice and studied their triglyceride and metabolic phenotypes when fed normal chow and high-fat diets. The effects of adipose and liver-specific ANGPTL4-deficiency on triglyceride and glucose homeostasis were determined after 12 weeks of high-fat feeding, as well as after 6 months of high-fat feeding to model a chronic state of obesity.

RESULTS

Effects of tissue-specific ANGPTL4 deficiency on plasma TG levels and TG uptake into tissues.

To examine the tissue-specific roles of ANGPTL4, we generated adipose- and liver-specific *Angptl4* knockout mice. First, we generated *Angptl4*-floxed mice (*Angptl4*$^{fl/fl}$) by utilizing CRISPR/Cas9 to insert LoxP sites in the introns between exons 1 and 2 and between exons 3 and 4 (**Figure 1A**). Recombination between LoxP sites generates a frame-shift resulting in a truncated (145 aa) protein in which the final 35 amino acids do not match the native sequence. Adipose-specific (*Angptl4*^{AdipoKO}) and liver-specific (*Angptl4*^{LivKO}) mice were generated by crossing *Angptl4*$^{fl/fl}$ mice with adiponectin-cre and albumin-cre mice, respectively. As expected, expression of *Angptl4* in gonadal, subcutaneous, and brown adipose tissues (gWAT, sWAT, BAT) was significantly reduced in *Angptl4*^{AdipoKO} mice, while being preserved in other tissues (**Figure 1B**). Likewise, in *Angptl4*^{LivKO} mice, *Angptl4* expression was significantly reduced only in the liver (**Figure 1C**). Fasting plasma triglyceride levels were significantly lower in 8-week-old male and female *Angptl4*^{AdipoKO} mice compared to *Angptl4*$^{fl/fl}$ mice (**Figure 1D**), whereas TG levels were not different in either male or female *Angptl4*^{LivKO} mice compared to *Angptl4*$^{fl/fl}$ mice (**Figure 1D**). These results suggest that the lower plasma TG levels observed in *Angptl4* whole-body knockout mice (2, 9, 12) is due to the loss of adipose-derived ANGPTL4. We observed a decrease in fasting plasma free fatty acid levels in *Angptl4*^{AdipoKO} male mice compared to *Angptl4*$^{fl/fl}$ mice, but no difference in free fatty acids levels in *Angptl4*^{LivKO} mice compared to *Angptl4*$^{fl/fl}$ mice

(**Figure 1E)**. There were no genotype-specific differences in fasting blood glucose levels between groups (**Figure 1F)**.

We previously observed increased plasma triglyceride clearance and increased adipose uptake of triglycerides in whole-body *Angptl4*$^{-/-}$ mice (9). In that study we hypothesized that the increased clearance was due to ANGPTL4 deficiency specifically in the adipose tissue (9). To determine if this was indeed the case, we performed triglyceride clearance assays on female *Angptl4*^{AdipoKO} and *Angptl4*^{LivKO} mice using radiolabeled chylomicrons. We also assessed uptake of radiolabeled chylomicrons into specific tissues. After an intravenous injection of radiolabeled chylomicrons, *Angptl4*^{AdipoKO} mice cleared the radiolabeled TGs from the plasma faster than *Angptl4*$^{fl/fl}$ mice (**Figure 2A**). The rate of radiolabeled clearance was also modestly increased in *Angptl4*^{LivKO} mice compared to *Angptl4*$^{fl/fl}$ mice. (**Figure 2B**). Similar to what we had observed with whole-body *Angptl4*$^{-/-}$ mice (9), *Angptl4*^{AdipoKO} female mice had increased radiolabeled uptake into adipose depots compared to *Angptl4*$^{fl/fl}$ mice (**Figure 2C**). No significant differences in tissue uptake were observed in female *Angptl4*^{LivKO} mice, other than a decrease in TG uptake in the quadriceps, (**Figure 2D)**. These data support our previous hypothesis that deficiency in adipose ANGPTL4, not liver ANGPTL4, is responsible for the increased triglyceride uptake into adipose tissue.

Effects of high-fat feeding on body phenotypes and plasma parameters in tissue-specific ANGPTL4-deficient mice.

Given the importance of ANGPTL4 in directing triglycerides away from adipose tissue (9), we sought to determine how high-fat feeding would alter metabolic phenotypes in *Angptl4*^{AdipoKO}, *Angptl4*^{LivKO}, and *Angptl4*$^{fl/fl}$ mice. We randomly assigned *Angptl4*^{AdipoKO}, *Angptl4*^{LivKO} and *Angptl4*$^{fl/fl}$ mice at 8 weeks of age to a normal chow (NCD) or high fat diet (HFD;60% kCal/fat) and fed them the respective diet for 12 weeks. On HFD, body weight gain was similar between all groups (**Figure 3A,B**); however, in this cohort, *Angptl4*^{LivKO} mice fed a normal chow diet gained slightly less weight than *Angptl4*$^{fl/fl}$ mice (**Figure 3B**). Adiposity, as determined by NMR, was greater in all mice fed a HFD compared to mice fed a NCD (**Figure 3C,D)**. Despite no differences in body weight, *Angptl4*^{AdipoKO} mice had significantly more total fat mass compared to *Angptl4*$^{fl/fl}$ mice when fed a NCD (**Figure 3C**). This genotype-specific difference in fat mass was not seen in HFD-fed *Angptl4*^{AdipoKO} mice, nor were any genotype-specific differences in fat mass observed in *Angptl4*^{LivKO} mice (**Figure 3C,D**). Moreover, no genotype-specific differences in specific tissue weights were observed in either *Angptl4*^{AdipoKO} or *Angptl4*^{LivKO} mice (**Supplemental Figure 1**).

Tissue expression of *Angptl4* was influenced both by genotype and by diet. As expected, expression of *Angptl4* in gonadal, subcutaneous and brown adipose tissues (eWAT, sWAT, BAT) was much lower in *Angptl4*^{AdipoKO} mice compared to *Angptl4*$^{fl/fl}$ mice (**Figure 3E**). Surprisingly, *Angptl4*^{AdipoKO} mice on NCD had greatly reduced *Angptl4* expression in the heart and moderately reduced expression in the liver compared to *Angptl4*$^{fl/fl}$ mice (**Figure 3E**), suggesting that loss of ANGPTL4 in the adipose tissue had a systemic effect leading to downregulation of ANGPTL4 in other tissues. In *Angptl4*^{LivKO} mice, expression of *Angptl4* was reduced only in the liver compared to *Angptl4*$^{fl/fl}$ mice (**Figure 3F**). Interestingly, HFD-alone significantly decreased *Angptl4* expression in several tissues, including the heart, liver and white adipose tissue (**Figure 3E,F**). These data indicate that high fat feeding can regulate expression of *Angptl4* even in absence of targeted tissue-specific loss of *Angptl4*.

As before, *Angptl4*^{AdipoKO} mice, but not *Angptl4*^{LivKO} mice fed a NCD had significantly lower fasting plasma TG levels compared to *Angptl4*$^{fl/fl}$ mice (**Figure 4A,B**). 12 weeks of HFD feeding lowered fasting TG levels in all groups and mostly negated the differences in plasma TG levels between *Angptl4*^{AdipoKO} and *Angptl4*$^{fl/fl}$ mice (**Figure 4A,B**). HFD feeding for 12 weeks decreased plasma non-esterified fatty

acid levels and increased plasma glucose and liver triglyceride levels in all groups, but there were no genotype specific differences on either NCD or HFD. (**Figure 4C–H**).

As changes in energy expenditure play a role in the pathogenesis of obesity, we asked if either liver or adipose-specific loss of ANGPTL4 would lead to changes in energy expenditure, oxygen consumption (VO_2), carbon dioxide production (VCO_2,) or respiratory quotient (RQ; VCO_2)/VO_2) Using the Promethion metabolic caging system, we observed no differences in energy expenditure, VO_2, VCO_2, or RQ in *Angptl4*^{AdipoKO} and *Angptl4*^{LivKO} mice on NCD compared to *Angptl4*$^{fl/fl}$ mice (**Supplemental Figure 2**). Interestingly, compared to floxed controls, increased energy expenditure was observed in the *Angptl4*^{LivKO} mice fed a HFD during both light and dark cycles. Both VO_2 and VCO_2 were increased in HFD-fed *Angptl4*^{LivKO} mice, while the RQ was unchanged. No differences were observed between *Angptl4*^{AdipoKO} and *Angptl4*$^{fl/fl}$ mice on HFD (**Supplemental Figure 2**).

Effects of high-fat feeding on TG uptake and LPL activity in tissue-specific *Angptl4* KO mice.

To assess if high-fat diet feeding altered triglyceride partitioning in an ANGPTL4-dependent manner, we performed plasma triglyceride clearance and tissue uptake assays on male *Angptl4*^{AdipoKO} and *Angptl4*^{LivKO} mice at the end of 12 weeks of either NCD or HFD feeding. On a NCD, *Angptl4*^{AdipoKO} mice cleared the radiolabeled TGs from the plasma faster than *Angptl4*$^{fl/fl}$ mice (**Figure 5A**), but no difference in triglyceride clearance was observed on a NCD for *Angptl4*^{LivKO} mice compared to *Angptl4*$^{fl/fl}$ mice (**Figure 5B**). Mice fed a HFD had faster clearance of plasma triglycerides than those fed a NCD, but on HFD there were no genotype specific differences in clearance rates (**Figure 5A,B**). Consistent with our observations in female mice, on NCD *Angptl4*^{AdipoKO} male mice had increased radiolabel uptake into epididymal and subcutaneous adipose depots compared to floxed controls (**Figure 5C**)**.** Interestingly, on HFD, the differences in radiolabel uptake into adipose tissues between *Angptl4*^{AdipoKO} mice and *Angptl4*$^{fl/fl}$ littermates were reduced (**Figure 5C**). No significant differences in tissue uptake were observed in male *Angptl4*^{LivKO} mice fed either a NCD or HFD compared to *Angptl4*$^{fl/fl}$ mice (**Figure 5D)**. These data again support the idea that on a NCD, deficiency in adipose ANGPTL4 results in increased triglyceride uptake into adipose tissue, but also suggest that this difference decreases in the face of high-fat feeding.

To elucidate whether the increased uptake of triglyceride-derived fatty acids into adipose tissue in *Angptl4*^{AdipoKO} mice was the result of increased LPL activity we measured tissue lipase activity. LPL activity was greater in the gonadal adipose tissue of *Angptl4*^{AdipoKO} mice on either NCD or HFD compared to *Angptl4*$^{fl/fl}$ mice (**Figure 6A**). There were no genotype specific differences in tissue LPL activity between *Angptl4*^{LivKO} mice and *Angptl4*$^{fl/fl}$ mice (**Figure 6B)**. HFD itself altered LPL activity in some tissues, increasing activity in quadriceps and slightly decreasing activity in epididymal white adipose tissue in both cohorts (**Figure 6A,B**). We also assessed if loss of ANGPTL4 resulted in changes in liver lipase activity. As expected, LPL activity in the liver was low compared to total lipase activity. We found no genotype specific differences in total lipase, hepatic lipase, or LPL activity on either diet (**Figure 6C–F**). We also measured tissue gene expression of *Lpl* and found no genotype-specific differences (**Supplemental Figure 3**). Together, TG clearance and LPL activity in *Angptl4*^{AdipoKO} mice closely resemble those we have previously reported in whole-body ANGPTL4 knockout mice (9), supporting the idea that the lack of adipose-derived ANGPTL4 is the primary driver of the increased adipose LPL activity and TG clearance.

Effects of high-fat feeding on glucose tolerance and insulin sensitivity in tissue-specific ANGPTL4-deficient mice.

A previous report found that an independent strain of adipose-specific ANGPTL4 knockout mice had improved glucose tolerance compared to wild-type mice after being fed a HFD for 4 weeks (10). To assess if the loss of adipose or liver-derived ANGPTL4 altered glucose metabolism in our mice, we performed glucose (GTT) and insulin tolerance (ITT) tests. On a normal chow diet, no differences were observed in glucose tolerance or insulin sensitivity in either *Angptl4*^{AdipoKO} or *Angptl4*^{LivKO} mice compared to floxed controls (**Figure 7)**. However, glucose tolerance and insulin sensitivity were markedly improved in HFD-fed Angptl4^{AdipoKO} mice compared to HFD-fed floxed controls (**Figure 7A,C**). The loss of liver-derived ANGPTL4 resulted in no improvements in glucose tolerance or insulin sensitivity on either diet (**Figure 7B,D**). These data support a protective role for loss of adipose-derived ANGPTL4 on systemic glucose homeostasis. Chronic inflammation has been linked with insulin resistance during obesity and type 2 diabetes (13). To test whether the changes we observed in glucose tolerance and insulin sensitivity were due to changes in tissue inflammation we measured tissue expression (liver, eWAT, sWAT and BAT) of inflammatory markers C-C Motif Chemokine Ligand 2 (*Ccl2), Cd68*, and tumor necrosis factor α (*Tnfα*). As expected, there was an increase in inflammation in all tested tissues of HFD-fed mice. However, no major genotype specific differences were observed (**Supplemental Figure 4**).

Effects of tissue specific ANGPTL4 deficiency in mice after a chronic high-fat diet.

To better characterize the role of ANGPTL4 in the setting of chronic obesity, we fed *Angptl4*^{AdipoKO}, *Angptl4*^{LivKO} and *Angptl4*$^{fl/fl}$ mice a NCD or HFD (60% kCal/fat) for 6 months. Initially, there were no genotype-specific differences in weight gain between any of the diet groups (**Figure 8A,B**). However, after 18 weeks on diet, the body weight curves began to diverge with *Angptl4*^{AdipoKO} mice gaining more weight than littermate *Angptl4*$^{fl/fl}$ mice on both a NCD or and a HFD (**Figure 8A**). At the end of 6 months of high-fat feeding, *Angptl4*^{LivKO} mice weighed slightly more than their high-fat fed *Angptl4*$^{fl/fl}$ controls (**Figure 8B**). Adiposity, as determined by NMR, was greater in all mice fed a HFD compared to mice fed a NCD, and there was an significant increase in total fat mass in the high fat fed *Angptl4*^{AdipoKO} mice compared to high fat fed *Angptl4*$^{fl/fl}$ controls (**Figure 8C,D**). There were no genotype specific differences in tissue weights (**Supplemental Figure 5**). As expected, expression of *Angptl4* in the gonadal, subcutaneous and brown adipose tissues (eWAT, sWAT, BAT) of *Angptl4*^{AdipoKO} mice and in the liver of *Angptl4*^{LivKO} mice were much lower than in *Angptl4*$^{fl/fl}$ littermates (**Figure 8E,F**). Similar to what we observed after 12 weeks of high-fat feeding, *Angptl4* expression was reduced in heart, liver, and epididymal white adipose tissue of Angptl4$^{fl/fl}$ mice fed a HFD for 6 months, again supporting the idea that *Angptl4* expression in these tissues is regulated by diet.

After 6 months on diet, *Angptl4*^{AdipoKO} mice fed a NCD continued to have significantly lower fasting plasma triglyceride levels compared to *Angptl4*$^{fl/fl}$ mice, but on a HFD these differences were not significant (**Figure 9A**). As before, no genotype-specific differences in plasma TG levels were observed between *Angptl4*^{LivKO} mice and *Angptl4*$^{fl/fl}$ controls (**Figure 9B**). At this age, ANGPTL4-deficiency in either adipose or liver had no significant effect on plasma non-esterified fatty acids, blood glucose, or liver triglycerides levels (**Figure 9C–H**). Interestingly, although HFD-fed mice had lower fasting plasma non-esterified free fatty acid levels than NCD-fed mice, at this time point, the diet induced differences in blood glucose and liver TG mostly disappeared (**Figure 9C–H**).

After 6 months on diet, *Angptl4*^{AdipoKO} mice continued to clear radiolabeled triglycerides from the plasma faster than littermate *Angptl4*$^{fl/fl}$ mice on NCD (**Figure 10A**). *Angptl4*^{AdipoKO} mice also cleared triglycerides faster when fed a HFD, though the difference was less pronounced (**Figure 10A**). No genotype-specific difference in radiolabeled clearance was observed in *Angptl4*^{LivKO} mice compared to littermate *Angptl4*$^{fl/fl}$ mice (**Figure 10B**). Again, *Angptl4*^{AdipoKO} male mice fed a NCD had increased uptake of radiolabeled fat into white adipose depots compared to floxed controls, but on HFD those

differences largely disappeared (**Figure 10C**). No genotype-specific differences in tissue radiolabeled uptake were observed in *Angptl4*^{LivKO} mice (**Figure 10D).**

To understand why adipose tissue deficiency no longer resulted in improved adipose clearance of triglycerides after a 6 month high-fat diet, we next measured tissue specific LPL activity. After 6 months of high-fat feeding, LPL activity was still greater in the adipose depots of *Angptl4*^{AdipoKO} mice compared to those of *Angptl4*$^{fl/fl}$ mice (**Figure 11A**). These data suggest that during the setting of obesity increased LPL activity in the adipose tissue of *Angptl4*^{AdipoKO} mice no longer leads to increased adipose triglyceride uptake. This may be because the capacity of white adipose tissues to store triglycerides has become the limiting factor for adipose storage rather than the rate of LPL lipolysis. There were no genotype specific differences in LPL activity in the *Angptl4*^{LivKO} mice compared to floxed control mice (**Figure 11B**). Similar to what was observed at the 12 week time point, there were no genotype-specific differences in total lipase, hepatic lipase, or LPL activity in the livers of either *Angptl4*^{AdipoKO} or *Angptl4*^{LivKO} mice (**Figure 11C–F**). We also measured tissue gene expression of *Lpl* and found no genotype-specific differences (**Supplemental Figure 6**).

Finally, we asked if the disappearance of improved adipose triglyceride clearance after 6 months on HFD had an effect on the improved glucose tolerance we had observed in *Angptl4*^{AdipoKO} mice after 12 weeks on HFD (see Figure 6). Indeed, we found that *Angptl4*^{AdipoKO} mice no longer had improved glucose tolerance after 6 months on HFD (**Figure 12A**). And while *Angptl4*^{AdipoKO} mice remained more insulin sensitive than *Angptl4*$^{fl/fl}$ mice after 6 months on HFD, the improvement was greatly reduced compared to that observed after 12 weeks of HFD (**Figure 12C**). Interestingly, despite no evidence of altered triglyceride partitioning, *Angptl4*^{LivKO} mice displayed improved glucose tolerance compared to littermate *Angptl4*$^{fl/fl}$ controls after 6 months of high-fat feeding (**Figure 12B**). Insulin sensitivity was also slightly, but not statistically significantly improved (**Figure 12D**). As before, we measured tissue expression (liver, eWAT, sWAT and BAT) of inflammatory markers *Ccl2, Cd68* and *Tnfα*. Once again, there was an increase in inflammation in HFD-fed mice in tested tissues, but no major genotype specific differences were observed (**Supplemental Figure 7**).

DISCUSSION

Proteins made and secreted by the liver (hepatokines) and adipose (adipokines) tissues play a vital role in lipid and glucose homeostasis during obesity. ANGPTL4 is highly expressed by both the adipose and liver in mice and humans (3, 14, 15). In this study we investigated the triglyceride phenotypes of adipose and liver-specific ANGPTL4 knockout mice. We also investigated how adipose or liver-specific loss of ANGPTL4 affected body weight, glucose tolerance, and insulin resistance in the setting of either 3 or 6 months of long-term high-fat diet feeding and obesity. We found that adipose-, but not liver-specific loss of ANGPTL4 resulted in lower plasma triglycerides and increased uptake of triglyceride-fatty acids into adipose tissue. We also found that for mice fed a high-fat diet, adipose-specific ANGPTL4 deletion initially resulted in improved glucose tolerance and insulin sensitivity, but over time this improvement disappeared. Conversely, liver-specific knockout mice initially showed no difference in glucose tolerance and insulin sensitivity, but after 6 months on HFD, these mice showed signs of improvement in both.

The role of ANGPTL4 in regulating triglyceride metabolism has been well established. Human carriers of the E40K mutation in ANGPTL4 have lower triglycerides and a lower risk of coronary artery disease (5) and dyslipidemia during obesity (8). In mice, genetic loss of ANGPTL4 leads to decreased fasting plasma TG levels and increased uptake of triglycerides into adipose tissue (3, 9). As plasma triglyceride clearance and partitioning is catalyzed by LPL, increased LPL activity due to the lack of inhibition by ANGPTL4 is almost certainly the cause of the lower triglyceride levels in ANGPTL4-

deficient mice and humans. Indeed, ANGPTL4-deficient mice have increased white adipose LPL activity, corresponding to the increase in triglyceride uptake in these tissues (9). The specific increase in adipose tissue LPL activity and TG uptake led us to previously postulate that adipose derived ANGPTL4 was likely responsible for the triglyceride phenotypes in whole-body ANGPTL4 knockout mice (9). Here, adipose-specific loss of ANGPTL4 in mice fed a chow diet phenocopies the triglyceride phenotypes observed in whole-body *Angptl4*$^{-/-}$ mice. *Angptl4*^{AdipoKO} mice had lower plasma triglyceride levels, increased uptake of triglycerides into adipose tissue, and increased adipose LPL activity. In contrast, liver-specific knockout of ANGPTL4 resulted in no discernable triglyceride phenotypes, at least under the conditions tested in this study. This was true in both male and female mice. The triglyceride phenotypes observed in *Angptl4*^{AdipoKO} mice were consistent with those recently reported by Aryal *et al.* using an independently derived adipose-specific ANGPTL4 knockout mouse (10). It is important to note that unlike the flox allele used by Aryal *et al,* which is predicted, after recombination, to yield a truncated ANGPTL4 containing the first 1-186 amino acid residues and may retain hypomorphic function (23), our allele does not yield a protein containing the LPL inhibitory domain. Both the current study and the Aryal *et al*. study support our previous hypothesis that it is primarily loss of adipose ANGPTL4 that is responsible for the alterations in plasma triglyceride levels and triglyceride partitioning observed in *Angptl4*$^{-/-}$ mice.

Angptl4$^{-/-}$ mice fed a high fat diet (HFD) develop a lethal intestinal injury and lymphatic nodule inflammation (11). This phenotype appears to be mediated by the lack of macrophage ANGPTL4, allowing excessive lipid uptake into lymphatic macrophages (11). Lethality on a high-fat diet was also observed with mice treated with an anti-ANGPTL4 antibody (16). A recent study found that the lethal intestinal phenotype seen in *Angptl4*$^{-/-}$ mice could be avoided by feeding the mice a diet high in unsaturated fatty acids and cholesterol accompanied by fructose in drinking water (17). On this diet, *Angptl4*$^{-/-}$ mice gained more weight and had higher mesenteric fat mass, but also had improved glucose tolerance (17). In our study, we used liver and adipose-specific ANGPTL4 conditional knockout mice to circumvent the high-fat feeding intestinal pathophysiology observed in whole-body knockout mice. Similar to *Angptl4*$^{-/-}$ mice fed a high unsaturated fat, high-fructose diet, we found that *Angptl4*^{AdipoKO} mice gained more weight than littermate controls. However, this increased weight gain was only observed in mice ~6 months old or older and was evident in both HFD-fed and chow fed mice. These data suggest that loss of adipose tissue ANGPTL4 does increase weight gain, albeit only moderately and only over long periods of time.

Loss of adipose ANGPTL4 in the context of HFD had an interesting effect on LPL activity and adipose triglyceride uptake. On a chow diet, the increase in adipose LPL activity in *Angptl4*^{AdipoKO} mice led to a corresponding increase in adipose-tissue uptake of triglycerides. This connection between LPL activity and triglyceride uptake in adipose was lost in mice fed a HFD. Adipose LPL activity remained higher in the adipose tissue of *Angptl4*^{AdipoKO} mice fed HFD compared to floxed control mice, but the enhanced adipose-tissue uptake observed on chow diet was largely lost. These data suggest that on a chronic high-fat diet, LPL activity is no longer rate-limiting for the entry of triglyceride-derived fatty acids into adipose. One possibility is that LPL continues to hydrolyze lipoprotein triglycerides at a higher rate in HFD-fed *Angptl4*^{AdipoKO} mice, but that uptake of the released fatty acids is not as efficient. The efficiency of fatty acid uptake following LPL lipolysis is known to vary in adipose tissue, resulting in spillover of NEFAs into the plasma (18). The mechanisms that account for the variation in uptake efficiency are not known, but could be the result of alterations in the expression of lipid transport, processing and storage-related proteins (e.g. CD36, FABP proteins) in the adipose tissues in the setting of HFD-feeding and adipose hypertrophy (21, 22).

High-fat feeding experiments performed by Janssen *et al*. (17), suggested that ANGPTL4 deficiency not only impacts triglyceride metabolism, but also glucose metabolism. Their work demonstrated that *Angptl4*$^{-/-}$ mice fed a diet rich in unsaturated fatty acids, gained more weight than wildtype mice, but had lower blood glucose levels and improved glucose tolerance. Indeed, human studies found that carriers of the inactivating E40K mutation in *Angptl4* had lower fasting glucose levels than non-diabetic participants (19). The same study also demonstrated that carriers of *Angptl4* loss-of-function variants had a lower odds ratio (0.89) for developing type 2 diabetes. Although it is tempting to attribute these improvements in glucose homeostasis to relief of LPL inhibition and improved triglyceride clearance to adipose, it has not yet been clearly demonstrated that this is this case. We found that after 12 weeks on HFD *Angptl4*^{AdipoKO} mice have improved glucose tolerance and are protected from insulin resistance. However, the improved glucose tolerance and protection from insulin resistance were mostly lost after long term HFD feeding. These observations are consistent with recent reports where independent strains of total adipose–specific or brown adipose-specific ANGPTL4 deficient mice demonstrated improved glucose tolerance after short-term HFD feeding (4 weeks), but lost these improvements after 20 weeks of HFD feeding (10, 20). The reason for the initial improvement and subsequent loss of glucose tolerance is unclear. We suspect that increasing TG partitioning to adipose improves glucose homeostasis, but that when the increased TG uptake to adipose is lost, as we observed in chronically HFD-fed mice, improved glucose tolerance is also lost. The therapeutic implications of these findings are not clear. Targeting ANGPTL4 to reduce plasma triglyceride levels while at the same time decreasing ectopic lipid deposition and improving glucose tolerance is an attractive idea (21). Here we show a reduction in fasting plasma triglyceride levels, enhanced adipose storage, and an improvement in glucose tolerance in *Angptl4*^{AdipoKO} mice, but these improvements faded after long term high-fat feeding. Aryal et al. reported similar observations (10). Thus, the long-term effectiveness of targeting ANGPTL4 to treat glucose tolerance remains in doubt.

A major question left unanswered in our study is the role of ANGPTL4 produced by the liver. Compared to littermate controls, we observed no differences in plasma triglyceride levels or triglyceride uptake levels in *Angptl4*^{LivKO} mice fed either HFD or normal chow. We also observed no differences in LPL activity, hepatic lipase activity, liver size, or liver triglycerides in these mice. Together these data suggest that liver ANGPTL4 does not play a major role in regulating hepatic or systemic triglyceride metabolism during fasting. Interestingly, we did find some evidence that liver ANGPTL4 does affect overall energy homeostasis. After 12 weeks on HFD, *Angptl4*^{LivKO} mice presented no improvements in glucose tolerance or insulin sensitivity compared to floxed controls, but after 6 months of HFD feeding, glucose tolerance was improved and there was a trend towards improved insulin sensitivity. These improvements occurred in the absence of differences in fasting plasma TG levels or alterations in tissue TG uptake. Moreover, metabolic caging data indicated that *Angptl4*^{LivKO} mice have increased energy expenditure. The mechanisms behind these improvements are unclear. Given that the improved glucose tolerance emerged only in mice fed a chronic HFD, it would be interesting to determine if an even longer period of HFD feeding would increase the difference in glucose tolerance between *Angptl4*^{LivKO} mice and controls and if the increased energy expenditure we observed in *Angptl4*^{LivKO} mice would persist at older ages.

The current study is not without limitations. We chose a 60% (kCal) high fat diet, a diet that is widely used experimentally to induce an obese and insulin resistant phenotype. Other diets may more closely reflect the typical American diet, such as the “Western diet” comprised of 42% (kCal) high fat, high sucrose and high cholesterol. Alternative diets that induce different pathological states might illuminate tissue-specific roles for ANGPTL4 that were missed in our study. Another limitation to our study is that we studied adipose- or liver-specific *Angptl4* knockout separately, but not in combination. Therefore, we would have missed any synergistic effects of ANGPTL4-deficiency in both tissues. Generating mice

that are deficient both in liver and adipose ANGPTL4 might allow for a greater interrogation of ANGPTL4's role in obesity, metabolic syndrome, and insulin resistance while circumventing the HFD-induced intestinal phenotype observed in whole body *Angptl4*$^{-/-}$ mice. ANGPTL4 is expressed, although at lower levels, in skeletal muscle and heart (22) and could have important actions during exercise (23) or situations of lipotoxicity (24). ANGPTL4 expressed in the intestine has also been implicated in the effects of the intestinal microbiota on metabolism (17). Generating additional tissue-specific *Angptl4* knockout mice could identify the roles of ANGPTL4 in these and other tissues.

Our studies highlight the importance of studying age and diet duration going forward. HFD studies in mice are generally performed in mice that are less than 1 year old and who have been fed a high-fat diet for 4 to 16 weeks. However, Aryal et al. clearly showed that adipose-specific ANGPTL4 knockout mice had greatly improved glucose tolerance after one month on HFD, but this improvement disappeared after 5 months on diet (10). We likewise show that *Angptl4*^{AdipoKO} mice have moderately improved glucose tolerance after 12 weeks on HFD diet, but little improvement, compared to control mice, after 6 months on diet. Moreover, while no improvement in glucose homeostasis was observed in our *Angptl4*^{LivKO} mice after 12 weeks of HFD feeding, after 6 months of HFD feeding, evidence of improved glucose tolerance began to emerge. Given that metabolic disease is most prevalent in older and obese populations, these observations highlight the need and importance of performing long-term feeding studies in aged mice if we are to fully understand the roles for different proteins in dyslipidemia and metabolic disease.

METHODS

Animals

Mice containing floxed alleles of the *Angptl4* gene were generated by the University of Iowa genome editing facility using Crispr/Cas9. B6SJLF1/J mice were purchased from Jackson Labs (100012; Bar Harbor, ME). Male mice older than 8 weeks were used to breed with 3-5 week old super-ovulated females to produce zygotes for microinjection. Female ICR (Envigo; Hsc:ICR(CD-1)) mice were used as recipients for embryo transfer. Chemically modified CRISPR-Cas9 crRNAs and CRISPR-Cas9 tracrRNAs were purchased from IDT (Alt-R® CRISPR-Cas9 crRNA; Alt-R® CRISPR-Cas9 tracrRNA (Cat# 1072532)). crRNA sequences were CCCTTTCACAGTCTGCTCTG and TGTGTCTAGTCTAGGAGCCG. The crRNAs and tracrRNA were suspended in T10E0.1 buffer (10 mM Tris pH 8, 0.1 mM EDTA) and combined to 1 µg/µl (~29.5 µM) final concentration in a 1:2 (µg:µg) ratio. The RNAs were heated at 98°C for 2 min and allowed to cool slowly to 20°C in a thermal cycler. The annealed cr:tracrRNAs were aliquoted to single-use tubes and stored at -80°C. Cas9 nuclease was also purchased from IDT (Alt-R® S.p. HiFi Cas9 Nuclease). Individual cr:tracr:Cas9 ribonucleoprotein complexes were made by combining Cas9 protein and cr:tracrRNA in T10E0.1 (final concentrations: 100 ng/ul (~0.6 µM) Cas9 protein and 100 ng/µl (~2.9 µM) cr:tracrRNA). The Cas9 protein and annealed RNAs were incubated at 37°C for 10 minutes. The two RNP complexes were mixed resulting in a final concentration of 100 ng/µl (~0.6 µM) Cas9 protein and 50 ng/µl (~1.5 µM) each cr:tracrRNA. Long single stranded DNA was prepared by digesting the Angptl4 target vector (524 bp 5' arm of homology; 911 bp floxed region; 636 bp 3' arm of homology) with the nicking enzyme Nb.Bsm1 (New England Biolabs) and purification from an alkaline-agarose gel. The final concentrations in the micro-injection mix were 20 ng/µl each cr:tracr RNA (~0.6 µM), 40 ng/µl Cas9 protein (~0.3 µM), and 10 ng/µl long ssDNA. Pronuclear-stage embryos were collected using methods described in (25). Embryos were collected in KSOM media (Millipore; MR101D) and washed 3 times to remove cumulous cells. Microinjection into the male pronucleus was performed and embryos incubated overnight. Two cell zygotes were implanted into pseudo-pregnant ICR females.

All pups were tested for the appropriate insertion of 5' and 3' LoxP sites by PCR amplification of the genomic region and subsequent sequencing. The above procedures resulted in the successful generation of a single male mouse with both 5' and 3' LoxP sites. This mouse was bred to a C57Bl/6 female mouse and the heterozygous progeny were interbred to generate homozygous floxed mice. During breeding, the presence of the LoxP Sites were confirmed by genotyping PCR using oligonucleotides TAGGCGCATCTACTAGGACTC (forward) and AGATATGCAAGGCTAGTGAAGAC (reverse) to detect the 5' LoxP site and oligonucleotides CCTCCAACATCTCTTGATGTAAC (forward) and ATATGTGTATGTGACTGGATGG (reverse) to detect the 3' LoxP site. Adipose-specific knockout mice (*Angptl4*^{AdipoKO}) were generated by breeding *Angptl4*$^{fl/fl}$ mice with C57/BL6 transgenic mice containing the adiponectin promoter-driven cre recombinase (kindly provided by Dr. Matthew Potthoff, Jackson stock 010803, (26)) Liver-specific knockout mice (*Angptl4*^{LivKO}) were generated by breeding *Angptl4*$^{fl/fl}$ mice with C57/BL6 transgenic mice containing the albumin promoter-driven cre recombinase (kindly provided by Dr. Eric Taylor, Jackson stock 003574, (27)) The presence of adiponectin-cre was verified by genotyping PCR using GGATGTGCCATGTGAGTCTG (forward) and ACGGACAGAAGCATTTTCCA (reverse) as primers. Primers used to confirm albumin-cre by genotyping PCR were TGCAAACATCACATGCACAC (forward to detect wildtype), GAAGCAGAAGCTTAGGAAGATGG (forward to detect Albumin Cre), and TTGGCCCCTTACCATAACTG (common reverse). In all studies Cre-negative *Angptl4*$^{fl/fl}$ littermates were used as controls.

All animal procedures were approved by the Institutional Animal Care and Use Committee at the University of Iowa and were carried out in accordance with the National Institute of Health *Guide for Care and Use of Laboratory Animals*. All animals were maintained in a climate-controlled environment at 25°C with a 12:12 hour light-dark cycle. Water was provided *ad libitum*. During non-fasting conditions mice were given standard mouse chow (NIH 7951) until 8 weeks of age when high-fat diet studies began. At 8 weeks of age mice were assigned to either remain on standard mouse chow (NIH 7951) or given high-fat diet (60% by kCal; Research Diets, 12592). Mice were fed their respective diets for either 12 weeks or 6 months.

Fasting Plasma Triglyceride, Free Fatty Acid and Glucose Analysis

Fasting plasma triglyceride, non-esterified fatty acid (NEFA), and glucose levels were measured in fasted (6 h) Angptl4$^{fl/fl}$, Angptl4^{LivKO}, and Angptl4^{AdipoKO} at 8 weeks of age before beginning diet studies and 12 weeks or 6 months following the start of diet studies. Blood was collected into EDTA-coated capillary tubes following a tail-nick and centrifuged to collect plasma (1,500xg, 15 minutes, 4ºC). For plasma TG analysis, plasma (2 ul, technical duplicates) was combined with Infinity^{TM-} Triglyceride Reagent (200 ul, Thermo Scientific TR22421) in a 96 well plate. Samples were incubated for 10 minutes at 37ºC, gently tapped to ensure proper mixing of reagent with sample and absorbance was read at 500 nm. Triglyceride concentrations were determined using a standard curve prepared from Triolein standard (Nu-Chek Prep, Lot T-235-N13-Y). For plasma NEFA analysis, plasma (2 ul, technical duplicates) was combined with Color Reagent A (112.5 ul, Wako HR Series NEFA-HR 999-34691/995-34791) and incubated for 10 minutes at 37ºC. Following incubation Color Reagent B was added to samples (37.5 ul, Wako HR Series NEFA-HR 991-34891/993-35191) and incubated for 5 minutes at 37ºC. Absorbance was read at 550 nm. Non-esterified fatty acid concentrations were determined using a standard curve prepared from Oleic Acid standard (TCI, O0180, Lot Z8RVM). Fasting plasma glucose concentration was measured using a glucometer (One Touch Ultra).

RNA Extraction and qPCR Analysis

Mouse tissues (heart, liver, epididymal white adipose tissue [eWAT], quadriceps muscle [quad], subcutaneous white adipose tissue [sWAT] and brown adipose tissue [BAT] were harvested following a 6 hour fast. Tissue was snap frozen in liquid nitrogen and stored at –80ºC until processed. Tissues were pulverized before homogenization. Total RNA was extracted using Trizol (Invitrogen) according to manufacturer's instructions. 2 µg of RNA was used to prepare cDNA with the High Capacity cDNA Reverse Transcription kit (Applied Biosystems, 4368813) according to manufacturer's instructions. Prepared cDNA was used for qPCR analysis using the following primers: *Angptl4* Forward: 3'-ATGACTTCAGATGGAGGCTGG, *Angptl4* Reverse: 3'-AATTGGCTTCCTCGGTTCCC-5', *LPL* Forward: 3'-CTGGTCTTAACCGGCCCAAT-5', *LPL* Reverse: 3'-TGCACATAGCCAGAAGGGTG-5', *U36B4* Forward: 3'-CGTCCTCGTTGGAGTGACA-5', *Ccl2* Forward-3'-CCCAATGAGTAGGCTGGAGA-5', *Ccl2* Reverse-3'-TCTGGACCCATTCCTTCTTG -5', *Cd68* Forward-3' GGGGCTCTTGGGAACTACAC-5', *Cd68* Reverse-3'- GTACCGTCACAACCTCCCTG-5', *Tnfα* Forward CCCTCACACTCAGATCATCTTCT-5', *Tnfα* Reverse-3'- GCTACGACGTGGGCTACAG-5' *U36B4* Reverse-3'-CGGTGCGTCAGGGATTG-5'. Prepared diluted cDNA, primers, and SYBR Green ER qPCR Supermix reagent (Invitrogen, 11762100) were combined, and PCR was performed on the QuantStudio 6 Flex system (Applied Biosystems, Iowa Institute of Human Genetics). Gene expression was calculated using the ΔΔct method using *U36B4* as the reference gene.

Preparation of ^{3}H-Labeled Chylomicrons

^{3}H-labeled chylomicrons were prepared as previously described (9). Briefly, glycosylphosphatidylinositol anchored high density lipoprotein binding protein 1 (GPIHBP1) knock out mouse (*Gpihbp1$^{-/-}$)* were orally gavaged with 100 µCi of [9,10-3H(N)]-Triolein (Perkin Elmer, NET431001MC) suspended in olive oil. After 4 h blood was collected via cardiac puncture. Blood was then combined with 0.5 M EDTA and centrifuged to collect plasma. Chylomicrons were isolated by centrifugation of plasma at 424,000 x g twice for 2 hours at 10ºC and collection of the upper layer. Chylomicrons were suspended in sterile saline and stored at 4ºC. Radioactivity was measured using a Beckman-Coulter Liquid Scintillation Counter.

Triglyceride Uptake Assay

TG clearance and uptake assays were performed in mice as previously described (9). Briefly, mice were fasted for 6 hours and then injected retro-orbitally with 100 ul of ^{3}H-labeled chylomicron suspension. Blood samples were taken 1, 5, 10, and 15 minutes after injection. For each time point, 10 µl of blood was assayed for radioactivity in BioSafe II scintillation fluid using a Beckman-Coulter Scintillation Counter. Following the final timepoint mice were anesthetized with isoflurane and perfused with 20 mL of cold 0.5% Tyloxapol in PBS solution. Tissues (heart, liver, kidney, eWAT, quad, sWAT and BAT) were harvested and weighed. 40-90 mg of each tissue was placed into a glass vial containing a 2:1 chloroform:methanol solution and stored overnight at 4ºC. 1 mL of 2 M $CaCl_2$ was added to each vial to separate the organic and aqueous phases. Samples were centrifuged for 10 minutes at 1,000 rpm and the upper aqueous layer was assayed for radioactivity in BioSafe II scintillation fluid using a Beckman-Coulter Scintillation Counter. The organic layer was allowed to evaporate overnight in an empty scintillation vial, then resuspended in scintillation fluid and counted. The counts per million (CPM) from the aqueous and organic fractions were combined to obtain the total uptake (CPM). To normalize radiolabel across mice, CPM values were normalized to the CPMs of the injected dose (measured by assaying 10% of the chylomicron suspension injected into the mouse).

Lipoprotein Lipase Activity Assays

LPL activity was measured as previously described (9). Briefly, frozen tissue samples were crushed using a metal tissue pulverizer. The tissue was resuspended in LPL assay buffer (25 mM NH_4Cl, 5 mM EDTA, 0.01% SDS, 45 U/mL heparin, 0.05% 3-(N,N-Dimethylmyristylammonio) propanesulfonate zwittergent detergent (Acros Organics, 427740050)) containing protease inhibitor (Mammalian ProteaseArrest-APExBIO K1008). The tissue was then vortexed and incubated on ice for 30 minutes with occasional further disruption with surgical scissors. The lysate was then clarified by centrifugation at 15,000 x g for 15 minutes (4°C). Protein concentrations were equalized prior to assaying activity. Supernatants were combined with a buffer comprised of 0.6 M NaCl, 80 mM Tris-HCl pH 8, 6% fatty-acid free BSA, and 1% of the EnzChek lipase fluorescent substrate (Molecular Probes, E33955). Fluorescence was measured (30 min, 37ºC) on a SpectraMax i3 plate reader (Molecular Devices). Relative lipase activity was determined following calculation of the linear slope of the curve and subtraction of background (assay buffer) slope readings. The assay was performed using duplicates of lysates. For liver lipase activity assays each substrate was treated with either vehicle (PBS) or NaCl (1M final concentration) to differentiate the roles of hepatic lipase (NaCl insensitive) from LPL (NaCl sensitive).

Glucose and Insulin Tolerance Tests

Glucose tolerance tests (GTT) were performed after fasting mice for 6 hours. Blood samples were collected before and 30, 60, 90 and 120 minutes following an intraperitoneal injection with glucose (12 week HFD study: 2g/kg for mice fed NCD, 1.3 g/kg for mice fed HFD; 6 month HFD study: 1g/kg for all mice). For mice fed a HFD for 12 weeks, blood was collected into an EDTA-coated capillary tube and stored on ice. Plasma was collected following centrifugation of sample tubes at 1,500xg for 20 minutes. Plasma glucose concentration was assessed using the Autokit Glucose kit (Wako-997-03001). 2.5 ul of plasma was combined with 200 ul of the Autokit glucose buffer solution and incubated at 37ºC for 5 minutes. Absorbance was read at 505 nM and 600 nM. The 600 nM reading was subtracted from the 505 nM read. Glucose concentrations were determined using a standard curve prepared from glucose standards provided by the kit. For mice fed a HFD for 6 months, blood glucose readings were taken following a tail nick, before injection and 30, 60, 90 and 120 minutes following glucose injection using a glucometer (OneTouch Ultra).

Insulin tolerance tests (ITT) were performed following a 4 h fast. Blood samples were collected via tail-nick before and 15, 30, 60 and 90 minutes after an intraperitoneal injection with insulin (0.75U/kg, Humalin-R 100). Glucose readings were taken immediately after each bleed using a glucometer (OneTouch Ultra).

Metabolic Cage Studies

Mice were individually housed in Promethion cage systems from Sable Systems International at the University of Iowa Metabolic Phenotyping Core. Mice were allowed to acclimate to their housing for 48 hours. Metabolic measurements were then taken for 48 hours. Measurements were taken during the duration of two light cycles (6 a.m.–6 p.m.) and two dark cycles (6 p.m.–6 a.m.). Measurements were recorded as energy expenditure (kcal/hr), oxygen consumption (VO_2 (ml/min)), carbon dioxide production (VCO_2 (ml/min)) and respiratory quotient (RQ, VCO_2/VO_2).

Body Composition

Body composition (fat, lean, fluid mass) was determined using nuclear magnetic resonance at 11 weeks of age in the 12-week diet challenge cohort and 25 weeks of age in the 6-month diet challenge cohort. Mice were weighed before being placed in a restraint tube without anesthesia and placed into

either a Bruker LF50 (for mice under 50 grams) or a Bruker LF90 (for mice over 50 grams). Following NMR scanning mice were immediately returned to their cages. Body composition measurements were performed in the Fraternal Order of the Eagles Diabetes Research Center Metabolic Phenotyping Core.

Statistics and Outlier Identification

Results are expressed as means ± SEM. Bar graphs also show individual values. Outlier identification was performed on all mouse datasets using ROUT analysis in GraphPad Prism. An unpaired Student's *t*-test was used to determine statistical significance of samples with two groups (Figures 1 and 2). For groups of three or more statistical significance was determined by 2-way ANOVA followed by multiple comparison with Tukey correction. Repeated measured ANOVA was utilized for chylomicron clearance, GTT, and ITT assays. Statistical analysis was performed in GraphPad Prism.

ACKNOWLEDGEMENTS

We thank the University of Iowa Genome Editing Facility for assistance in generating the ANGPTL4 floxed allele and the Fraternal Order of Eagles Diabetes Research Center Metabolic Phenotyping Core Laboratory for assistance is collecting metabolic caging data.

REFERENCES

1. Ge, H., J.-Y. Cha, H. Gopal, C. Harp, X. Yu, J. J. Repa, and C. Li. 2005. Differential regulation and properties of angiopoietin-like proteins 3 and 4. *J. Lipid Res.* **46**: 1484–1490.

2. Köster, A., Y. B. Chao, M. Mosior, A. Ford, P. A. Gonzalez-DeWhitt, J. E. Hale, D. Li, Y. Qiu, C. C. Fraser, D. D. Yang, J. G. Heuer, S. R. Jaskunas, and P. Eacho. 2005. Transgenic angiopoietin-like (angptl)4 overexpression and targeted disruption of angptl4 and angptl3: regulation of triglyceride metabolism. *Endocrinology*. **146**: 4943–4950.

3. Kersten, S., S. Mandard, N. S. Tan, P. Escher, D. Metzger, P. Chambon, F. J. Gonzalez, B. Desvergne, and W. Wahli. 2000. Characterization of the Fasting-induced Adipose Factor FIAF, a Novel Peroxisome Proliferator-activated Receptor Target Gene. *J. Biol. Chem.* **275**: 28488–28493.

4. Yoshida, K., T. Shimizugawa, M. Ono, and H. Furukawa. 2002. Angiopoietin-like protein 4 is a potent hyperlipidemia-inducing factor in mice and inhibitor of lipoprotein lipase. *J. Lipid Res.* **43**: 1770–1772.

5. Dewey, F. E., V. Gusarova, C. O'Dushlaine, O. Gottesman, J. Trejos, C. Hunt, C. V. Van Hout, L. Habegger, D. Buckler, K.-M. V. Lai, J. B. Leader, M. F. Murray, M. D. Ritchie, H. L. Kirchner, D. H. Ledbetter, J. Penn, A. Lopez, I. B. Borecki, J. D. Overton, J. G. Reid, D. J. Carey, A. J. Murphy, G. D. Yancopoulos, A. Baras, J. Gromada, and A. R. Shuldiner. 2016. Inactivating variants in ANGPTL4 and risk of coronary artery disease. *N. Engl. J. Med.* **374**: 1123–1133.

6. Myocardial Infarction Genetics and CARDIoGRAM Exome Consortia Investigators, N. O. Stitziel, K. E. Stirrups, N. G. D. Masca, J. Erdmann, P. G. Ferrario, I. R. König, P. E. Weeke, T. R. Webb, P. L. Auer, U. M. Schick, Y. Lu, H. Zhang, M.-P. Dube, A. Goel, M. Farrall, G. M. Peloso, H.-H. Won, R. Do, E. van Iperen, S. Kanoni, J. Kruppa, A. Mahajan, R. A. Scott, C. Willenberg, P. S. Braund, J. C. van Capelleveen, A. S. F. Doney, L. A. Donnelly, R. Asselta, P. A. Merlini, S. Duga, N. Marziliano, J. C. Denny, C. M. Shaffer, N. E. El-Mokhtari, A. Franke, O. Gottesman, S. Heilmann, C. Hengstenberg, P. Hoffman, O. L. Holmen, K. Hveem, J.-H. Jansson, K.-H. Jöckel, T. Kessler, J. Kriebel, K. L. Laugwitz, E. Marouli, N. Martinelli, et al. 2016. Coding variation in ANGPTL4, LPL, and SVEP1 and the risk of coronary disease. *N. Engl. J. Med.* **374**: 1134–1144.

7. Lotta, L. A., I. D. Stewart, S. J. Sharp, F. R. Day, S. Burgess, J. Luan, N. Bowker, L. Cai, C. Li, L. B. L. Wittemans, N. D. Kerrison, K.-T. Khaw, M. I. McCarthy, S. O'Rahilly, R. A. Scott, D. B. Savage, J. R. B. Perry, C. Langenberg, and N. J. Wareham. 2018. Association of Genetically Enhanced Lipoprotein Lipase–Mediated Lipolysis and Low-Density Lipoprotein Cholesterol–Lowering Alleles With Risk of Coronary Disease and Type 2 Diabetes. *JAMA Cardiol*. **3**: 957–966.

8. Bailetti, D., L. Bertoccini, R. M. Mancina, I. Barchetta, D. Capoccia, E. Cossu, A. Pujia, A. Lenzi, F. Leonetti, M. G. Cavallo, S. Romeo, and M. G. Baroni. 2019. ANGPTL4 gene E40K variation protects against obesity-associated dyslipidemia in participants with obesity. *Obes Sci Pract*. **5**: 83–90.

9. Cushing, E. M., X. Chi, K. L. Sylvers, S. K. Shetty, M. J. Potthoff, and B. S. J. Davies. 2017. Angiopoietin-like 4 directs uptake of dietary fat away from adipose during fasting. *Mol Metab*. **6**: 809–818.

10. Aryal, B., A. K. Singh, X. Zhang, L. Varela, N. Rotllan, L. Goedeke, B. Chaube, J.-P. Camporez, D. F. Vatner, T. L. Horvath, G. I. Shulman, Y. Suárez, and C. Fernández-Hernando. 2018. Absence of

ANGPTL4 in adipose tissue improves glucose tolerance and attenuates atherogenesis. *JCI Insight*. **3**: e97918.

11. Lichtenstein, L., F. Mattijssen, N. J. de Wit, A. Georgiadi, G. J. Hooiveld, R. van der Meer, Y. He, L. Qi, A. Köster, J. T. Tamsma, N. S. Tan, M. Müller, and S. Kersten. 2010. Angptl4 protects against severe proinflammatory effects of saturated fat by inhibiting fatty acid uptake into mesenteric lymph node macrophages. *Cell Metab.* **12**: 580–592.

12. Lee, E.-C., U. Desai, G. Gololobov, S. Hong, X. Feng, X.-C. Yu, J. Gay, N. Wilganowski, C. Gao, L.-L. Du, J. Chen, Y. Hu, S. Zhao, L. Kirkpatrick, M. Schneider, B. P. Zambrowicz, G. Landes, D. R. Powell, and W. K. Sonnenburg. 2009. Identification of a new functional domain in angiopoietin-like 3 (ANGPTL3) and angiopoietin-like 4 (ANGPTL4) involved in binding and inhibition of lipoprotein lipase (LPL). *J. Biol. Chem.* **284**: 13735–13745.

13. Xu, H., G. T. Barnes, Q. Yang, G. Tan, D. Yang, C. J. Chou, J. Sole, A. Nichols, J. S. Ross, L. A. Tartaglia, and H. Chen. 2003. Chronic inflammation in fat plays a crucial role in the development of obesity-related insulin resistance. *J Clin Invest*. **112**: 1821–1830.

14. Fagerberg, L., B. M. Hallström, P. Oksvold, C. Kampf, D. Djureinovic, J. Odeberg, M. Habuka, S. Tahmasebpoor, A. Danielsson, K. Edlund, A. Asplund, E. Sjöstedt, E. Lundberg, C. A.-K. Szigyarto, M. Skogs, J. O. Takanen, H. Berling, H. Tegel, J. Mulder, P. Nilsson, J. M. Schwenk, C. Lindskog, F. Danielsson, A. Mardinoglu, A. Sivertsson, K. von Feilitzen, M. Forsberg, M. Zwahlen, I. Olsson, S. Navani, M. Huss, J. Nielsen, F. Ponten, and M. Uhlén. 2014. Analysis of the human tissue-specific expression by genome-wide integration of transcriptomics and antibody-based proteomics. *Mol. Cell Proteomics*. **13**: 397–406.

15. Yoon, J. C., T. W. Chickering, E. D. Rosen, B. Dussault, Y. Qin, A. Soukas, J. M. Friedman, W. E. Holmes, and B. M. Spiegelman. 2000. Peroxisome Proliferator-Activated Receptor γ Target Gene Encoding a Novel Angiopoietin-Related Protein Associated with Adipose Differentiation. *Mol. Cell. Biol.* **20**: 5343–5349.

16. Desai, U., E.-C. Lee, K. Chung, C. Gao, J. Gay, B. Key, G. Hansen, D. Machajewski, K. A. Platt, A. T. Sands, M. Schneider, I. Van Sligtenhorst, A. Suwanichkul, P. Vogel, N. Wilganowski, J. Wingert, B. P. Zambrowicz, G. Landes, and D. R. Powell. 2007. Lipid-lowering effects of anti-angiopoietin-like 4 antibody recapitulate the lipid phenotype found in angiopoietin-like 4 knockout mice. *Proc. Natl. Acad. Sci. U.S.A.* **104**: 11766–11771.

17. Janssen, A. W. F., S. Katiraei, B. Bartosinska, D. Eberhard, K. Willems van Dijk, and S. Kersten. 2018. Loss of angiopoietin-like 4 (ANGPTL4) in mice with diet-induced obesity uncouples visceral obesity from glucose intolerance partly via the gut microbiota. *Diabetologia*. **61**: 1447–1458.

18. Evans, K., G. C. Burdge, S. A. Wootton, M. L. Clark, and K. N. Frayn. 2002. Regulation of Dietary Fatty Acid Entrapment in Subcutaneous Adipose Tissue and Skeletal Muscle. *Diabetes*. **51**: 2684–2690.

19. Gusarova, V., C. O'Dushlaine, T. M. Teslovich, P. N. Benotti, T. Mirshahi, O. Gottesman, C. V. Van Hout, M. F. Murray, A. Mahajan, J. B. Nielsen, L. Fritsche, A. B. Wulff, D. F. Gudbjartsson, M. Sjögren, C. A. Emdin, R. A. Scott, W.-J. Lee, A. Small, L. C. Kwee, O. P. Dwivedi, R. B. Prasad, S. Bruse, A. E. Lopez, J. Penn, A. Marcketta, J. B. Leader, C. D. Still, H. L. Kirchner, U. L. Mirshahi, A. H. Wardeh, C.

M. Hartle, L. Habegger, S. N. Fetterolf, T. Tusie-Luna, A. P. Morris, H. Holm, V. Steinthorsdottir, P. Sulem, U. Thorsteinsdottir, J. I. Rotter, L.-M. Chuang, S. Damrauer, D. Birtwell, C. M. Brummett, A. V. Khera, P. Natarajan, M. Orho-Melander, J. Flannick, L. A. Lotta, C. J. Willer, et al. 2018. Genetic inactivation of ANGPTL4 improves glucose homeostasis and is associated with reduced risk of diabetes. *Nat Commun*. **9**: 2252.

20. Singh, A. K., B. Aryal, B. Chaube, N. Rotllan, L. Varela, T. L. Horvath, Y. Suárez, and C. Fernández-Hernando. 2018. Brown adipose tissue derived ANGPTL4 controls glucose and lipid metabolism and regulates thermogenesis. *Mol Metab*. **11**: 59–69.

21. Davies, B. S. J. 2018. Can targeting ANGPTL proteins improve glucose tolerance? *Diabetologia*. **61**: 1277–1281.

22. Yue, F., Y. Cheng, A. Breschi, J. Vierstra, W. Wu, T. Ryba, R. Sandstrom, Z. Ma, C. Davis, B. D. Pope, Y. Shen, D. D. Pervouchine, S. Djebali, R. E. Thurman, R. Kaul, E. Rynes, A. Kirilusha, G. K. Marinov, B. A. Williams, D. Trout, H. Amrhein, K. Fisher-Aylor, I. Antoshechkin, G. DeSalvo, L.-H. See, M. Fastuca, J. Drenkow, C. Zaleski, A. Dobin, P. Prieto, J. Lagarde, G. Bussotti, A. Tanzer, O. Denas, K. Li, M. A. Bender, M. Zhang, R. Byron, M. T. Groudine, D. McCleary, L. Pham, Z. Ye, S. Kuan, L. Edsall, Y.-C. Wu, M. D. Rasmussen, M. S. Bansal, M. Kellis, C. A. Keller, C. S. Morrissey, et al. 2014. A comparative encyclopedia of DNA elements in the mouse genome. *Nature*. **515**: 355–364.

23. Chang, H., O. Kwon, M.-S. Shin, G. M. Kang, Y. H. Leem, C. H. Lee, S. J. Kim, E. Roh, H.-K. Kim, B.-S. Youn, and M.-S. Kim. 2018. Role of Angptl4/Fiaf in exercise-induced skeletal muscle AMPK activation. *Journal of Applied Physiology*. **125**: 715–722.

24. Yu, X., S. C. Burgess, H. Ge, K. K. Wong, R. H. Nassem, D. J. Garry, A. D. Sherry, C. R. Malloy, J. P. Berger, and C. Li. 2005. Inhibition of cardiac lipoprotein utilization by transgenic overexpression of Angptl4 in the heart. *PNAS*. **102**: 1767–1772.

25. Pinkert, C. A. 2002. Transgenic Animal Technology: A Laboratory Handbook. 2 edition. Academic Press, Amsterdam ; Boston.

26. Eguchi, J., X. Wang, S. Yu, E. E. Kershaw, P. C. Chiu, J. Dushay, J. L. Estall, U. Klein, E. Maratos-Flier, and E. D. Rosen. 2011. Transcriptional control of adipose lipid handling by IRF4. *Cell Metab*. **13**: 249–259.

27. Postic, C., M. Shiota, K. D. Niswender, T. L. Jetton, Y. Chen, J. M. Moates, K. D. Shelton, J. Lindner, A. D. Cherrington, and M. A. Magnuson. 1999. Dual Roles for Glucokinase in Glucose Homeostasis as Determined by Liver and Pancreatic β Cell-specific Gene Knock-outs Using Cre Recombinase. *J. Biol. Chem.* **274**: 305–315.

Figures

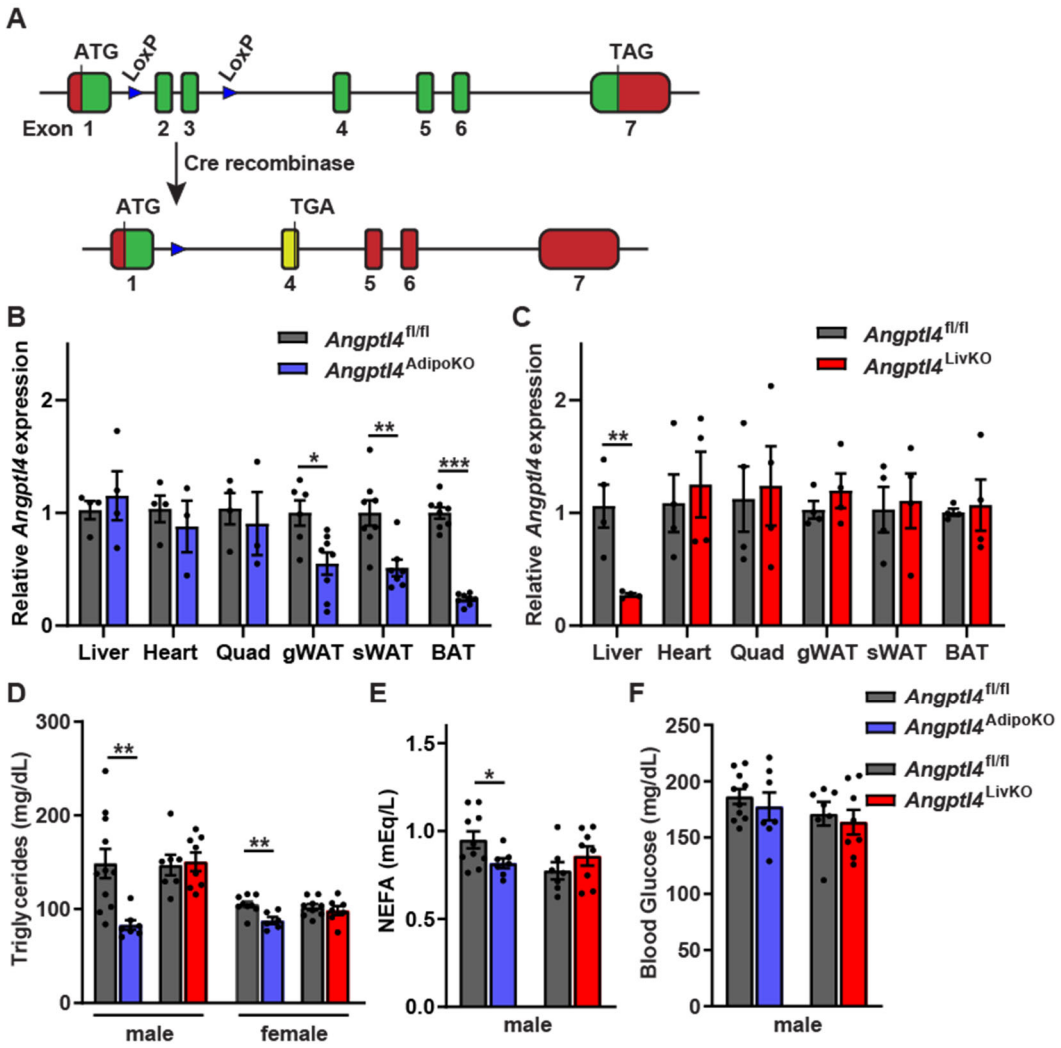

Figure 1. Generation and characterization of mice with adipose or liver-specific deletion of *Angptl4*. A) Schematic illustration of the lox-P sites in the *Angptl4*$^{fl/fl}$ allele and genomic rearrangement that results from Cre-mediated recombination. **B and C)** mRNA expression of *Angptl4* in liver, heart, quadriceps muscle (quad), gonadal white adipose tissue (gWAT), subcutaneous white adipose tissue (sWAT), and brown adipose tissues (BAT) of 8-12 week old male and female *Angptl4*$^{fl/fl}$, *Angptl4*^{AdipoKO} (B) and *Angptl4*^{LivKO} (C) mice following a 6 h fast (mean ± SEM; n=4-8). **D–F)** Fasting plasma triglyceride (D), non-esterified fatty acids (E) and blood glucose levels (F) in 8-12 week male and female (TG only) *Angptl4*$^{fl/fl}$, *Angptl4*^{AdipoKO} and *Angptl4*^{LivKO} mice following a 6 h fast. Bars represent mean ± SEM (n=7-11). *p<0.05, **p < 0.01, ***p<0.001. vs. *Angptl4*$^{fl/fl}$ mice by student t-test.

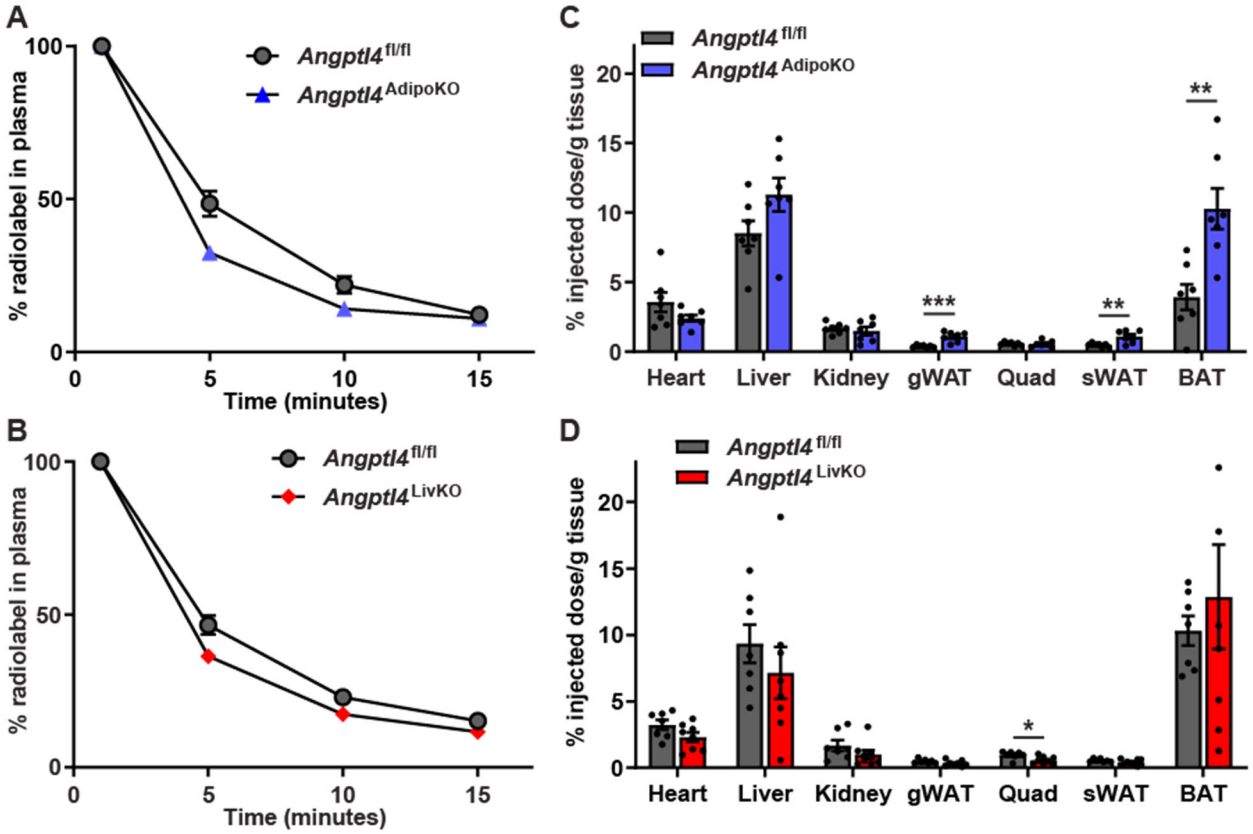

Figure 2. Chylomicron clearance and uptake in female *Angptl4*^{AdipoKO} and *Angptl4*^{LivKO} mice. Fasted (6 h) female *Angptl4*^{AdipoKO} (A,C) and *Angptl4*^{LivKO} (B,D) mice were injected intravenously with ^{3}H-triglyceride containing chylomicrons. **A and B)** Clearance of radiolabel from the plasma 1, 5, 10, and 15 min after injection. Points represent percentage of radiolabel remaining in the plasma at the indicated time points compared to the 1 min time point (mean±SEM; n=7-8). **C and D)** Uptake of radiolabel after 15 min (% injected dose/g tissue) into the indicated tissues (mean±SEM; n=7-8). *p<0.05, **p<0.01, ***p<0.001 vs. *Angptl4*$^{fl/fl}$ mice by student t-test.

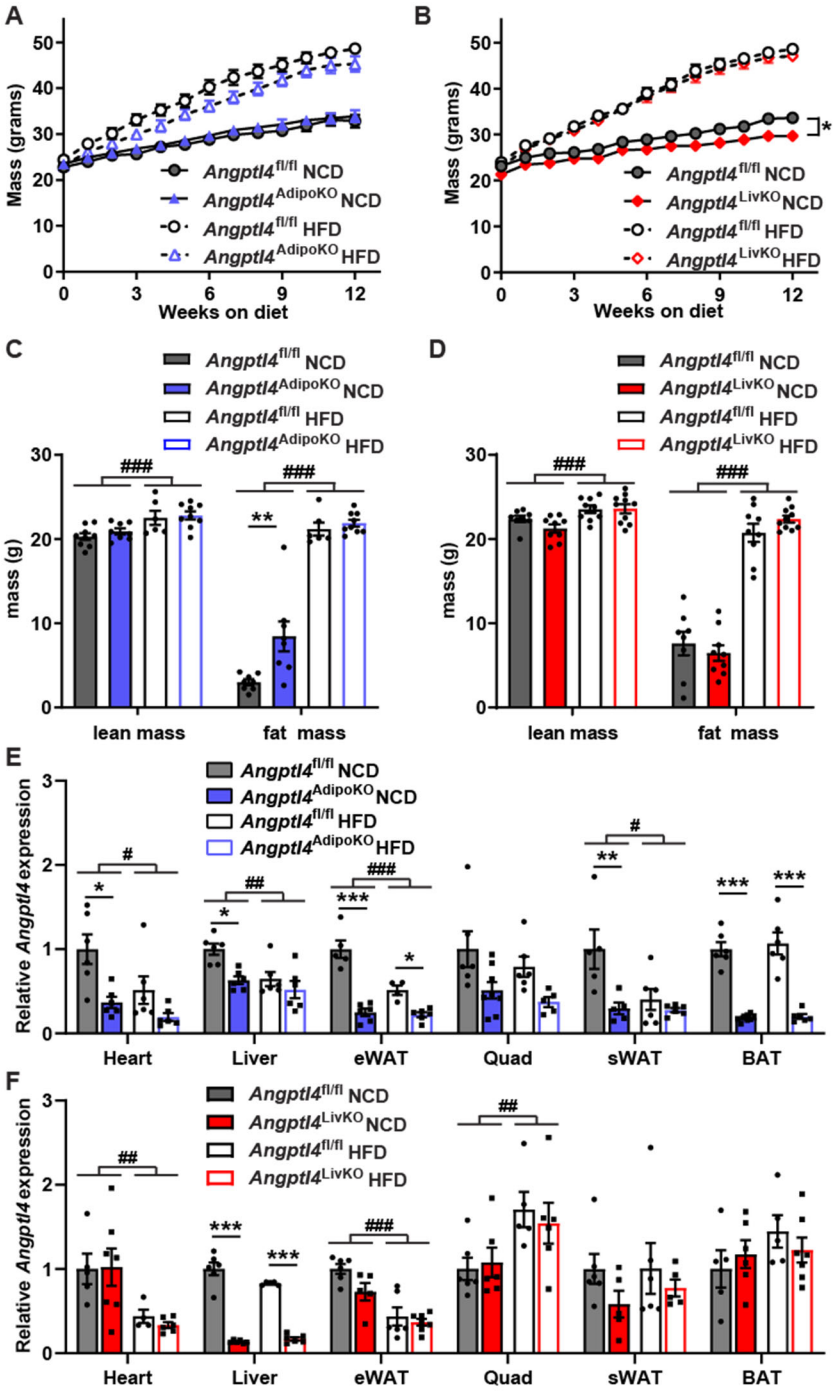

Figure 3. Body weights, fat mass, and *Angptl4* expression in *Angptl4*^{AdipoKO} and *Angptl4*^{LivKO} mice. A and B) Weekly body weights of male *Angptl4*^{AdipoKO} (A) and *Angptl4*^{LivKO} (B) mice fed either a normal chow diet (NCD) or a high fat diet (HFD; 60% by kCal) for 12 weeks starting at 8 weeks of age (mean±SEM; n=12-20/group). *p<0.05 by repeated measures ANOVA. **C and D)** Lean muscle and fat mass of *Angptl4*^{AdipoKO} (C) and *Angptl4*^{LivKO} (D) mice as measured by NMR after 12 weeks on diet (mean±SEM; n=6-9/group). **E and F)** mRNA expression of *Angptl4* from heart, liver, gonadal white adipose tissue (eWAT), quadriceps muscle (quad), subcutaneous white adipose tissue (sWAT), and brown adipose tissue (BAT) of fasted (6 h) male *Angptl4*^{AdipoKO} (E) and *Angptl4*^{LivKO} (F) mice after 12 weeks on diet (mean± SEM; n=4-8/group). #p<0.05, ##p<0.01, ###p<0.001 for dietary differences by two-way ANOVA. *p<0.05, **p<0.01, ***p<0.001 for individual genotype-specific differences by multiple comparison after two-way ANOVA (Tukey correction).

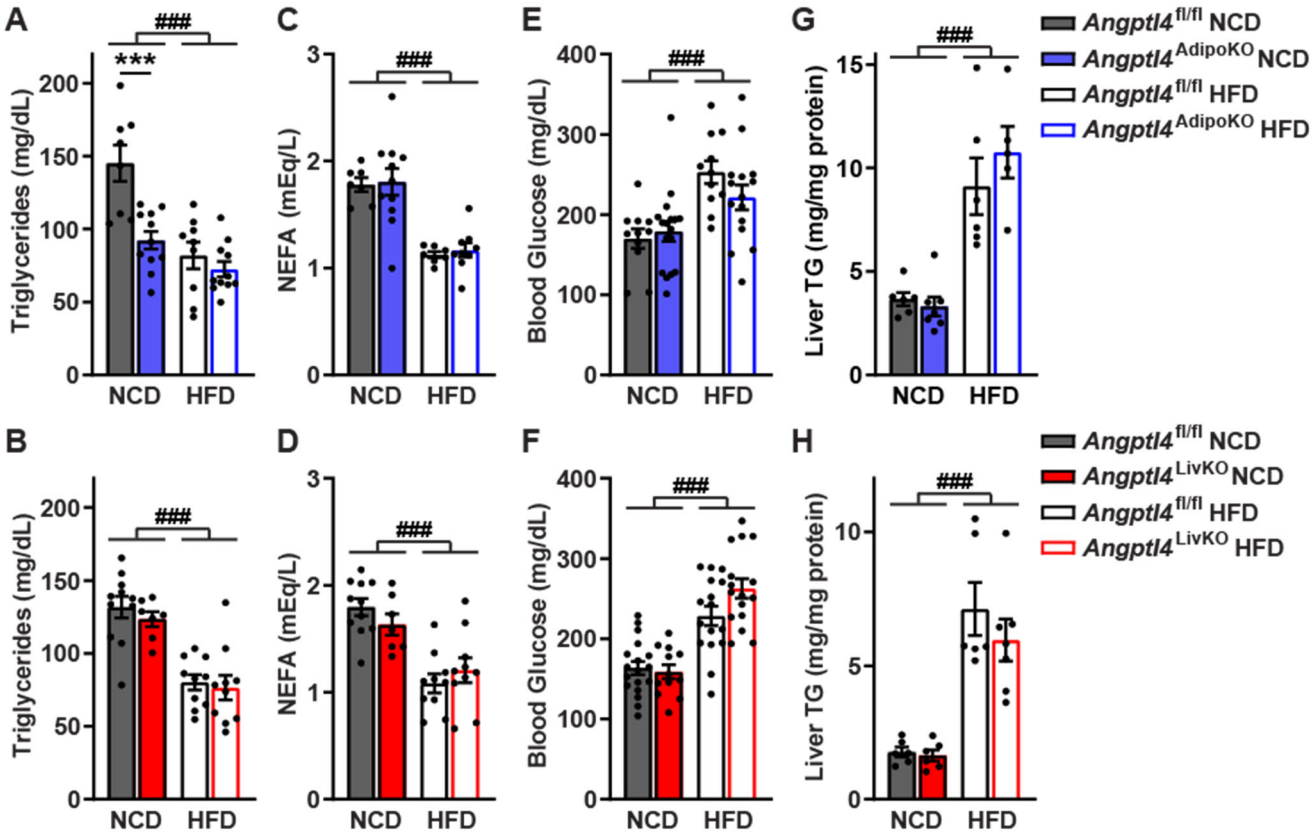

Figure 4. Metabolic phenotypes of *Angptl4*^{AdipoKO} and *Angptl4*^{LivKO} mice. Plasma triglycerides **(A,B)**, plasma non-esterified fatty acids **(C,D)**, blood glucose **(E,F),** and liver triglycerides **(G,H)** of fasted (6 h) male *Angptl4*^{AdipoKO} and *Angptl4*^{LivKO} mice at the end of 12 weeks of either normal chow diet (NCD) or high fat diet (HFD; mean±SEM; n=8-22 for A-F and n=4-7/group for G-H). ###p<0.001 for dietary differences by two-way ANOVA. ***p<0.001 for individual genotype-specific differences by multiple comparison after two-way ANOVA (Tukey correction).

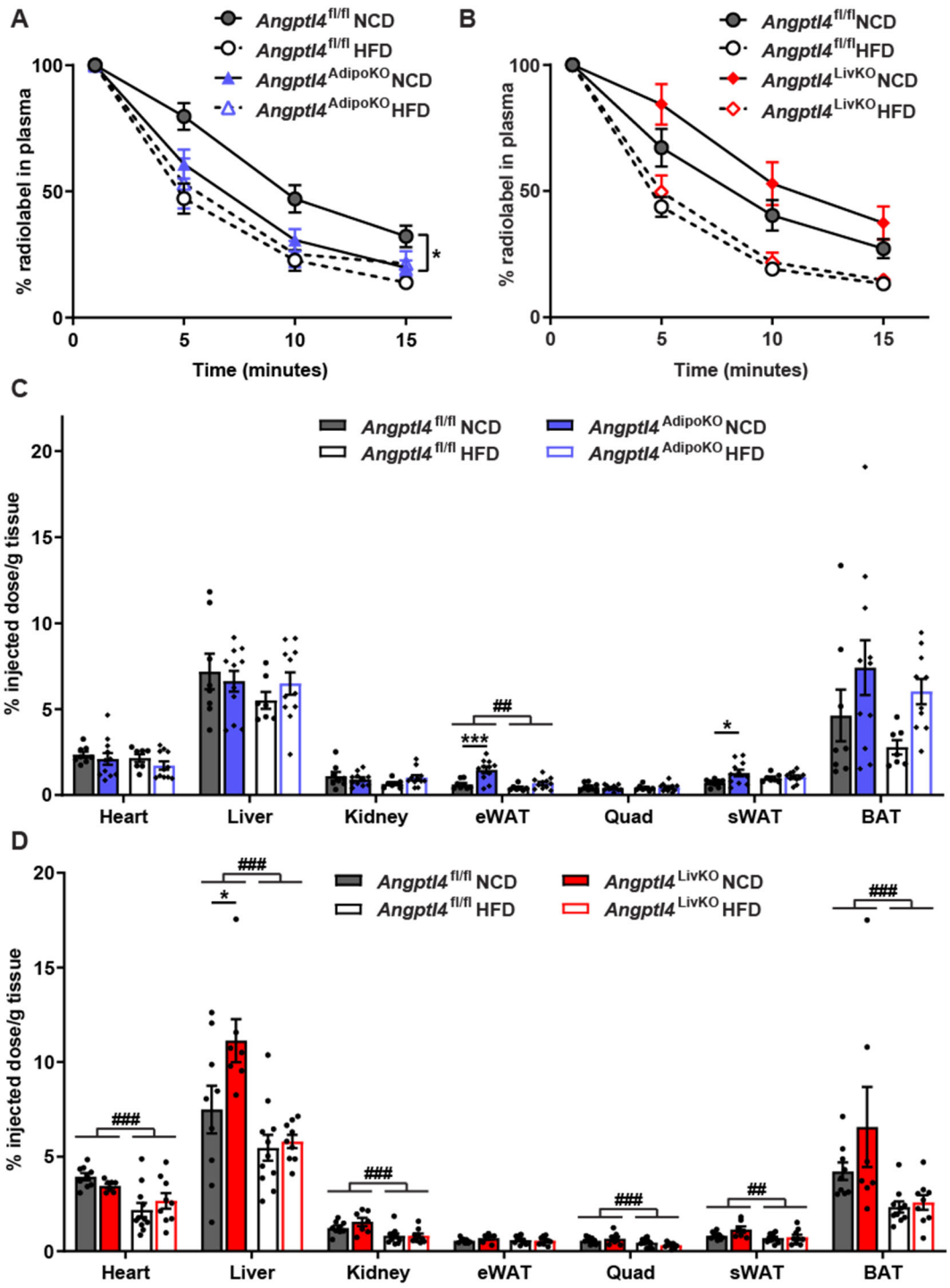

Figure 5. Chylomicron clearance and uptake in *Angptl4*^{AdipoKO} and *Angptl4*^{LivKO} mice. At the conclusion of 12 weeks of either normal chow diet (NCD) or high fat diet (HFD) *Angptl4*^{AdipoKO} (A,C) and *Angptl4*^{LivKO} (B,D) mice (n=7-10/group) were fasted (6 h) and injected intravenously with 3H-triglyceride containing chylomicrons. **A and B)** Clearance of radiolabel from the plasma 1, 5, 10, and 15 minutes after injection. Points represent percentage of radiolabel remaining in the plasma at the indicated time points compared to the 1 minute time point (mean±SEM). *p<0.05 by repeated measures ANOVA. **C and D)** Uptake of radiolabel (% injected dose/g tissue) into the indicated tissues after 15 min (mean±SEM). ##p<0.01, ###p<0.001 for dietary differences by two-way ANOVA. *p<0.05, ***p<0.001 for individual genotype-specific differences by multiple comparison after two-way ANOVA (Tukey correction).

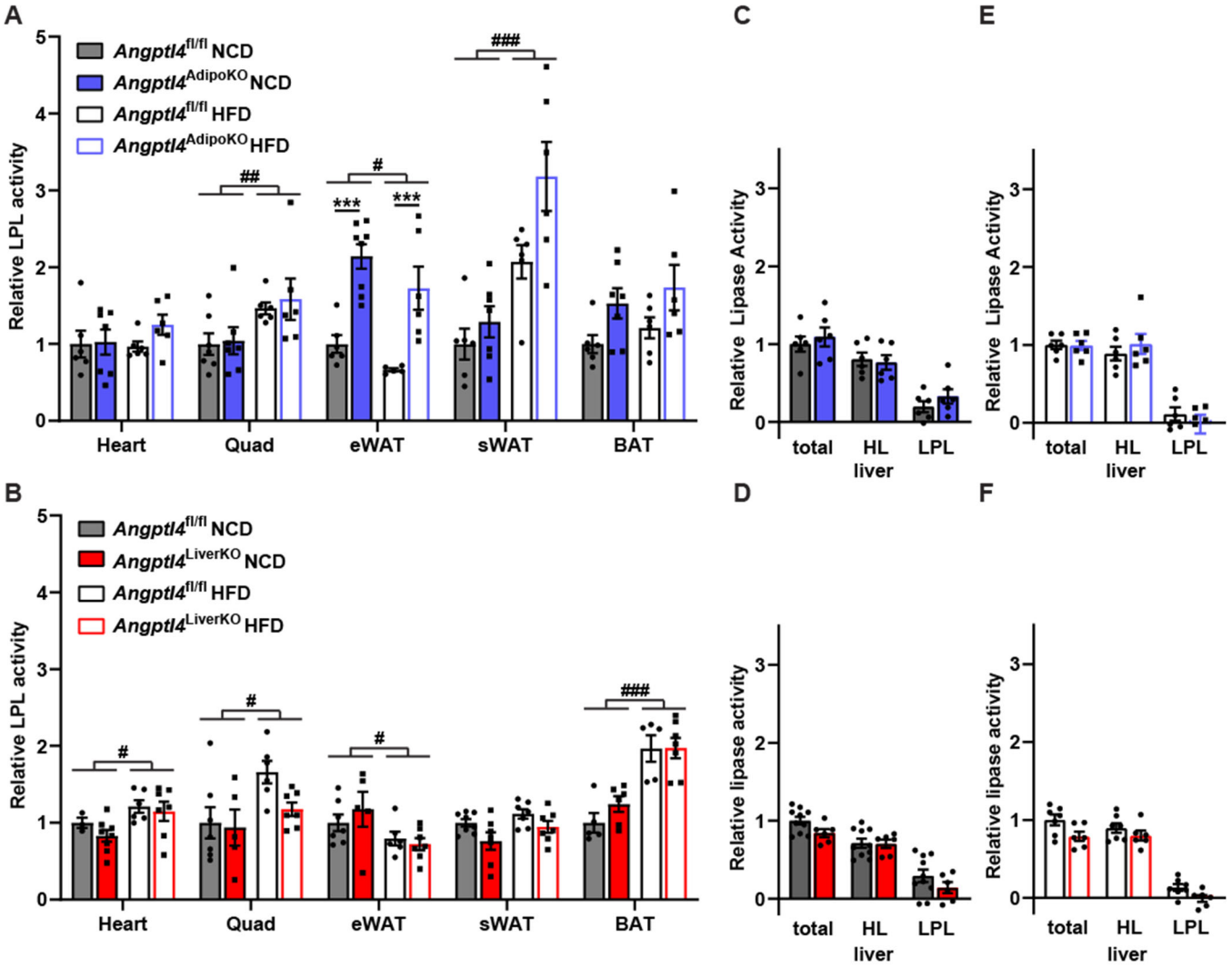

Figure 6. Lipase Activity in *Angptl4*^{AdipoKO} and *Angptl4*^{LivKO} mice. A and B) Heart, epididymal adipose tissue (eWAT), quadricep muscle (Quad), subcutaneous adipose tissue (sWAT), and brown adipose (BAT) tissue from fasted (6 h) male *Angptl4*^{AdipoKO} (A) and *Angptl4*^{LivKO} (B) mice were harvested and lipase activity was measured (n=3-7/group). **C–F**) Liver was harvested from fasted (6 h) male *Angptl4*^{AdipoKO} (C, NCD groups and E, HFD groups) and *Angptl4*^{LivKO} (D, NCD groups and F, HFD groups) mice (n=4-7/group). Lipase activity was measured in the presence or absence of 1M-NaCl to distinguish between hepatic and lipoprotein lipase. Bars show relative lipase activity in each tissue normalized to *Angptl4*$^{fl/fl}$ (mean±SEM). #p<0.05, ##p<0.01, ###p<0.001 for dietary differences by two-way ANOVA. ***p<0.001 for individual genotype-specific differences by multiple comparison after two-way ANOVA (Tukey correction).

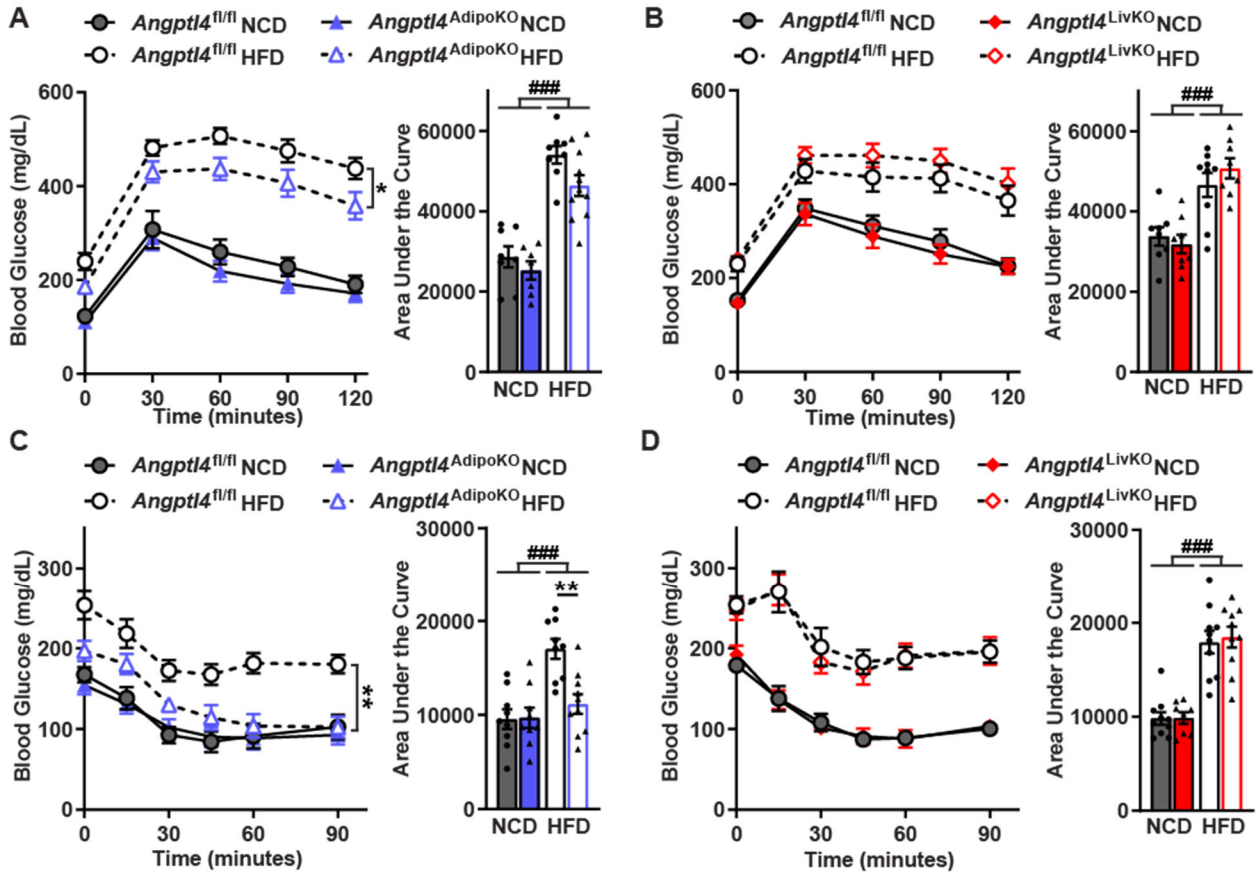

Figure 7. Glucose tolerance and insulin sensitivity of *Angptl4*^{AdipoKO} and *Angptl4*^{LivKO} mice. A and B) Glucose tolerance tests were performed on fasted (6 h) male *Angptl4*^{AdipoKO} (A) and *Angptl4*^{LivKO} (B) mice after 11 weeks of either a normal chow diet (NCD) or high fat diet (HFD). Mice were injected with glucose (2 g/kg for NCD; 1.3 g/kg HFD) and blood glucose concentrations were measured over 2 hours. Points represent glucose levels (mean±SEM; n=7-11) at each respective time point. Bar graphs represent area under the curve (mean±SEM) for all time points. *p<0.05 by repeated measures ANOVA. **C and D**) Insulin tolerance tests were performed on fasted (4 h) male *Angptl4*^{AdipoKO} (C) and *Angptl4*^{LivKO} (D) mice after 12 weeks of either a normal chow diet (NCD) or high fat diet (HFD). Mice were injected with 0.75 U/ml of human insulin (Humalin-R) and blood glucose concentrations were measured over 90 min. Points represent glucose levels (mean±SEM; n=7-11) at each respective time point. Bar graphs represent area under the curve (mean±SEM) for all time points. ###p<0.001 for dietary differences by two-way ANOVA. *p<0.05, **p<0.01, for individual genotype-specific differences by repeated measures ANOVA.

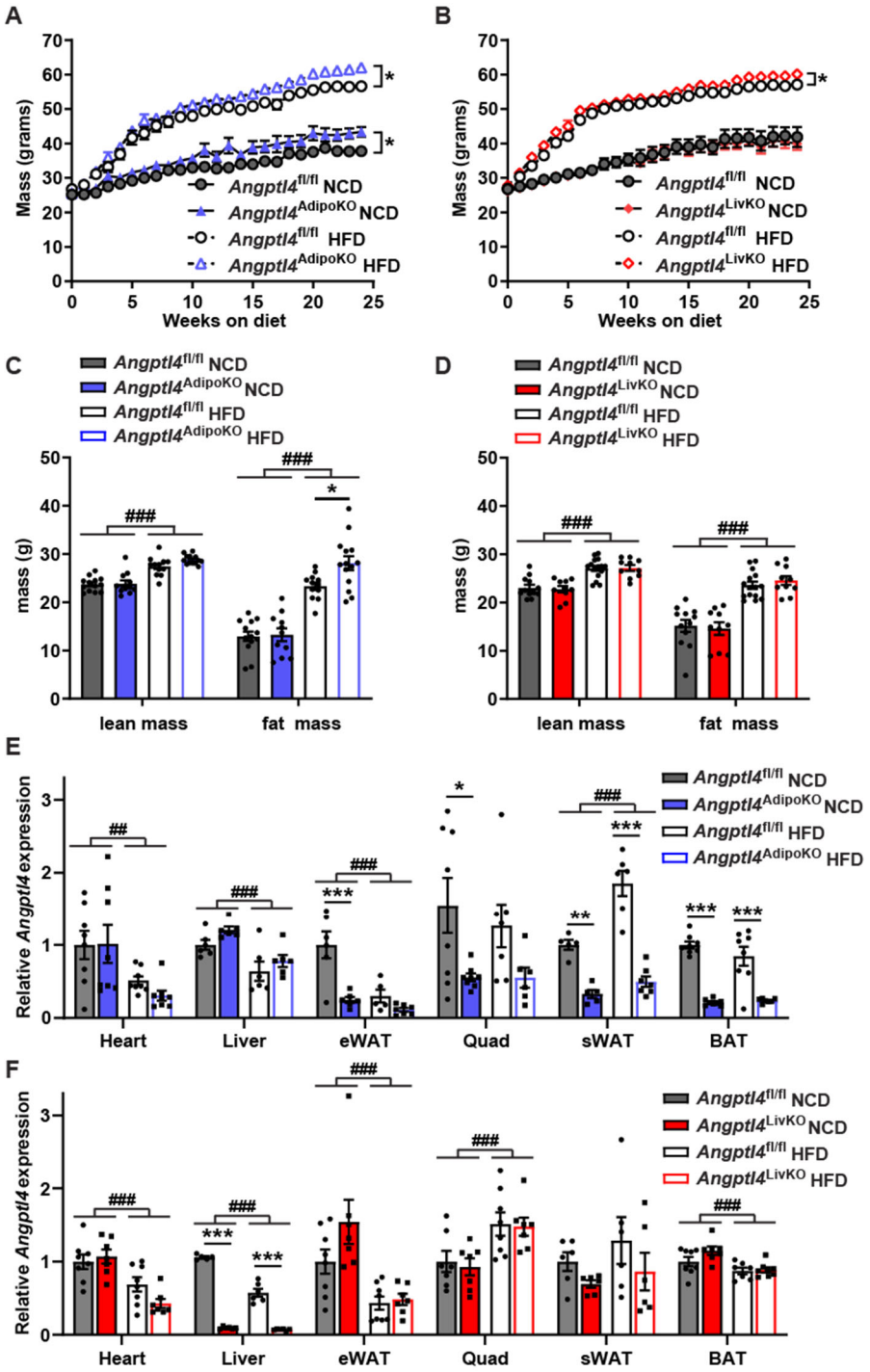

Figure 8. Body weights, fat mass, and *Angptl4* expression of *Angptl4*^{AdipoKO} and *Angptl4*^{LivKO} mice after chronic high-fat feeding. A and B) Weekly body weights of male *Angptl4*^{AdipoKO} (A) and *Angptl4*^{LivKO} (B) mice fed either a normal chow diet (NCD) or high fat diet (HFD) for 6 months starting at 8 weeks of age (mean±SEM; n=15-20/group). *p<0.05 by repeated measures ANOVA. **C and D)** Lean muscle and fat mass of *Angptl4*^{AdipoKO} (C) and *Angptl4*^{LivKO} (D) mice as measured by NMR after 24 weeks on diet. (mean±SEM; n=10-13/group). **E and F)** mRNA expression of *Angptl4* from heart, liver, gonadal white adipose tissues (eWAT), quadriceps muscle (quad), subcutaneous white adipose tissue (sWAT), and brown adipose tissues (BAT) of fasted (6 h) male *Angptl4*^{AdipoKO} (E) and *Angptl4*^{LivKO} *(F)* mice after 6 months on diet (mean± SEM; n=5-8/group). ##p<0.01, ###p<0.001 for dietary differences by two-way ANOVA. *p<0.05,***p<0.001 for individual genotype-specific differences by multiple comparison after two-way ANOVA (Tukey correction).

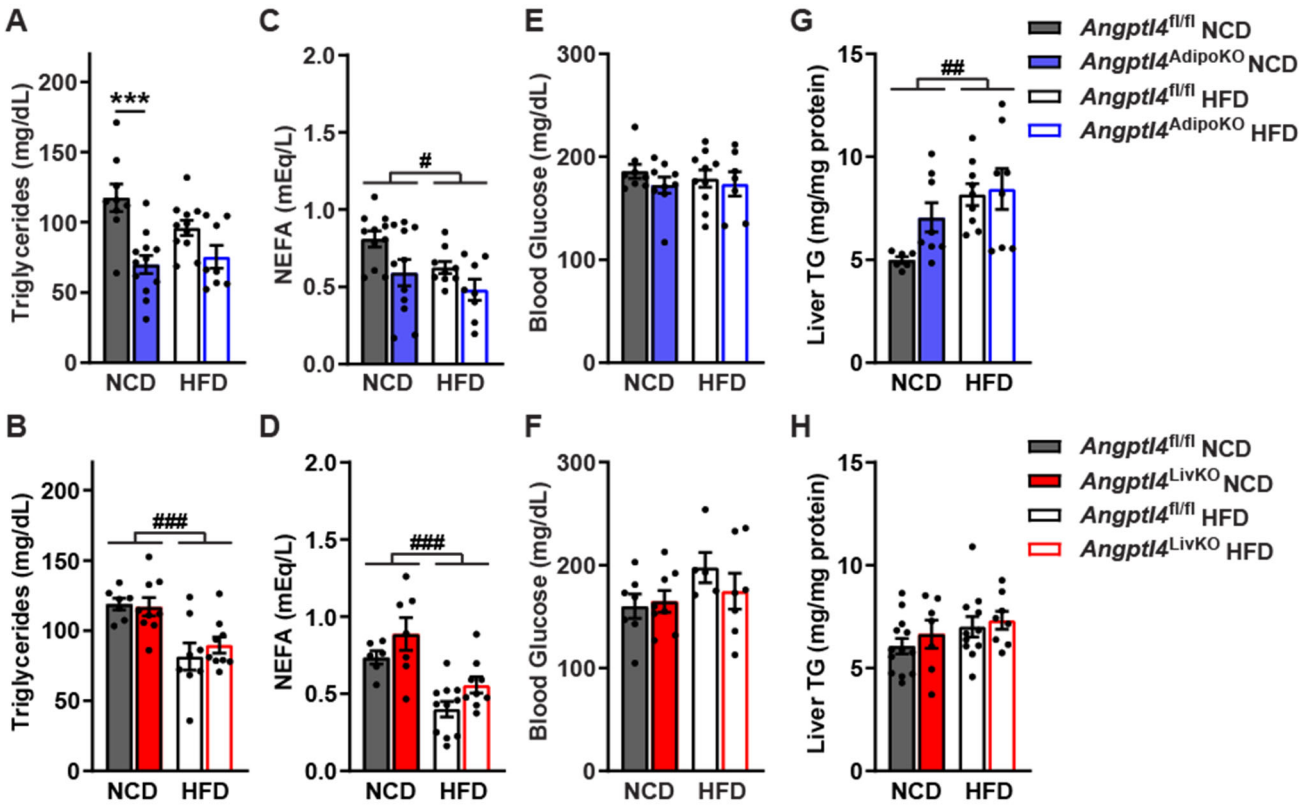

Figure 9. Metabolic phenotypes of *Angptl4*^{AdipoKO} and *Angptl4*^{LivKO} mice after chronic high-fat feeding. Plasma triglycerides **(A,B)**, plasma non-esterified fatty acids **(C,D)**, blood glucose **(E,F),** and liver triglycerides **(G,H)** of fasted (6 h) male *Angptl4*^{AdipoKO} and *Angptl4*^{LivKO} mice after 6 months of either normal chow diet (NCD) or a high fat diet (HFD) feeding (mean±SEM; n=7-12/group). #p<0.05, ##p<0.01, ###p<0.001 for dietary differences by two-way ANOVA. ***p<0.001 for individual genotype-specific conditions by multiple comparison after two-way ANOVA (Tukey correction).

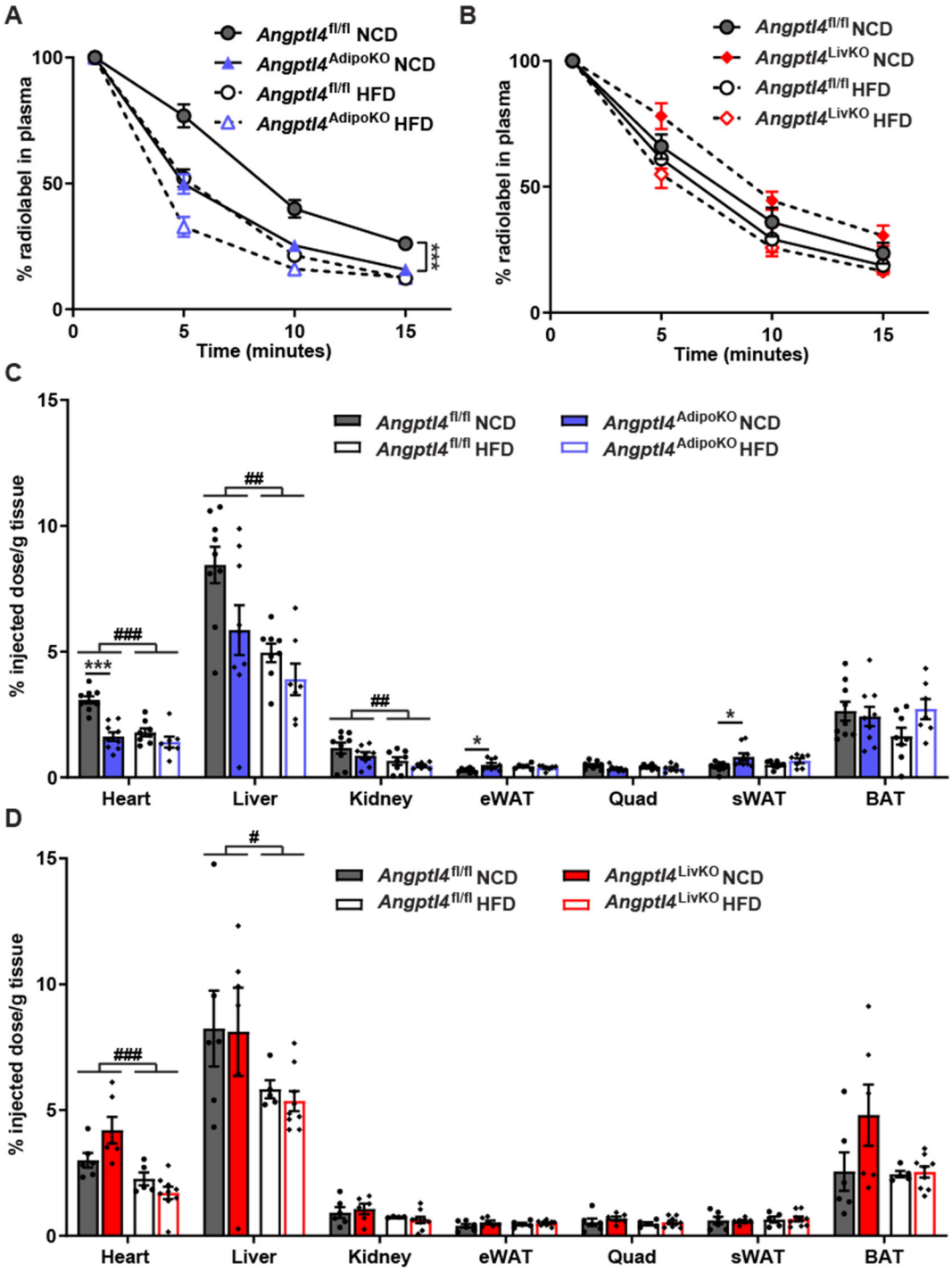

Figure 10. Chylomicron clearance and uptake in *Angptl4*^{AdipoKO} and *Angptl4*^{LivKO} mice after chronic high-fat feeding. At the conclusion of 6 months of either normal chow diet (NCD) or high fat diet (HFD) *Angptl4*^{AdipoKO} (A,C) and *Angptl4*^{LivKO} (B,D) mice (n=5-9/group) were fasted (6 h) and injected intravenously with 3H-triglyceride containing chylomicrons. **A and B)** Clearance of radiolabel from the plasma 1, 5, 10, and 15 minutes after injection. Points represent percentage of radiolabel remaining in the plasma at the indicated time points compared to the 1-minute time point (mean±SEM). ***p<0.001 by repeated measures ANOVA. **C and D)** Uptake of radiolabel (% injected dose/g tissue) into the indicated tissues after 15 min (mean±SEM). ##p<0.01, ###p<0.001 for dietary differences by two-way ANOVA. *p<0.05, ***p<0.001 for individual genotype-specific differences by multiple comparison after two-way ANOVA.

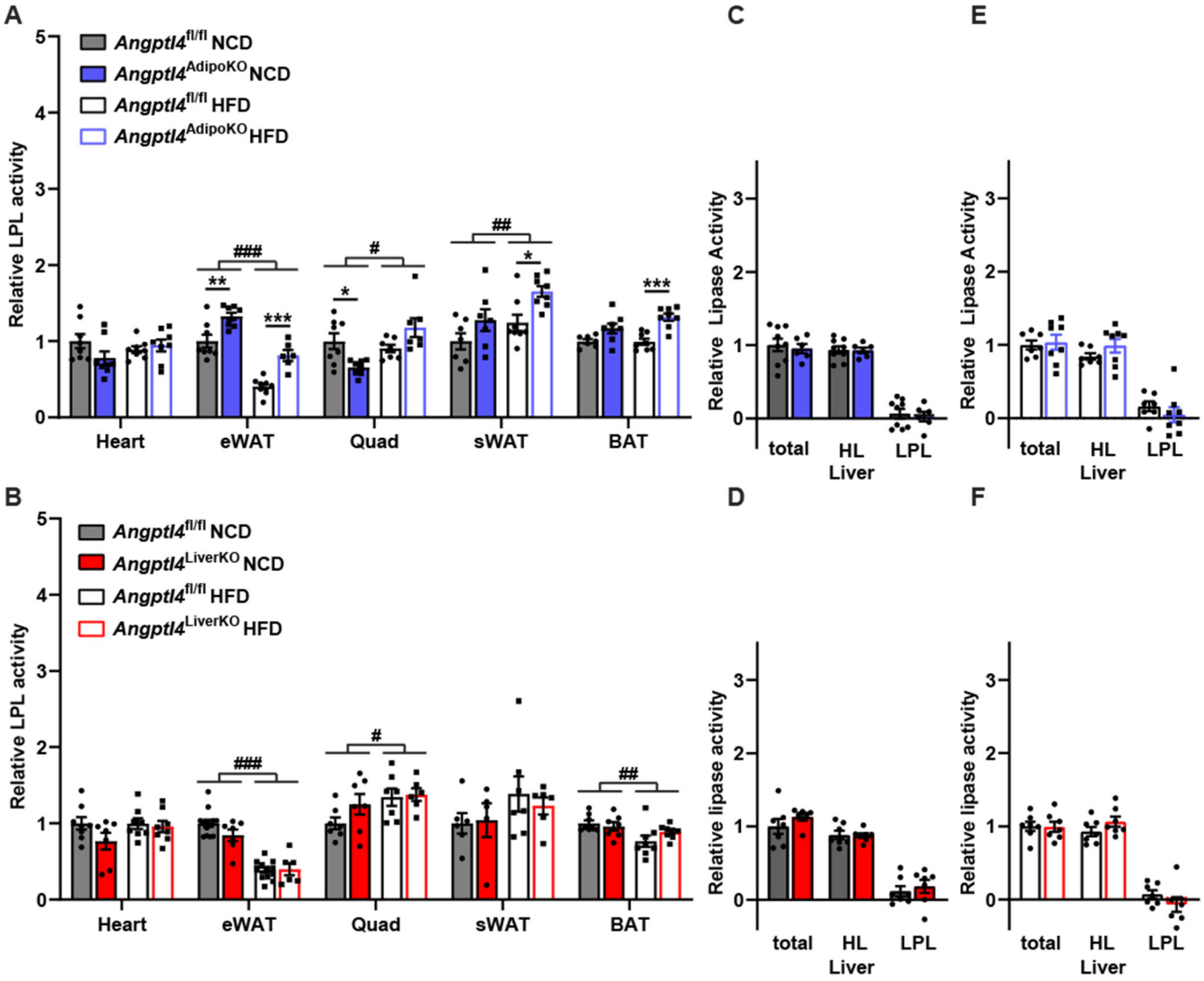

Figure 11. Lipase Activity *Angptl4*^{AdipoKO} and *Angptl4*^{LivKO} mice after chronic high fat feeding. A and B) Heart, epididymal adipose tissue (eWAT), Quadricep muscle (Quad), subcutaneous adipose tissue (sWAT), and brown adipose (BAT) tissue) from fasted (6 h) male *Angptl4*^{AdipoKO} (A) and *Angptl4*^{LivKO} (B) mice (n=4-13/group) were harvested and lipase activity was measured. **C–F)** Liver was harvested from fasted (6 h) male *Angptl4*^{AdipoKO} (C, NCD groups and E, HFD groups) and *Angptl4*^{LivKO} (D, NCD groups and F, HFD groups) mice (n=6-8/group). Lipase activity was measured in the presence or absence of 1M NaCl to distinguish between hepatic and lipoprotein lipase. Bars show relative lipase activity in each tissue normalized to *Angptl4*$^{fl/fl}$ (mean±SEM). #p<0.05, ##p<0.01, ###p<0.001 for dietary differences by two-way ANOVA. *p<0.05, **p<0.01, ***p<0.001 for individual genotype-specific differences by multiple comparison after two-way ANOVA (Tukey correction).

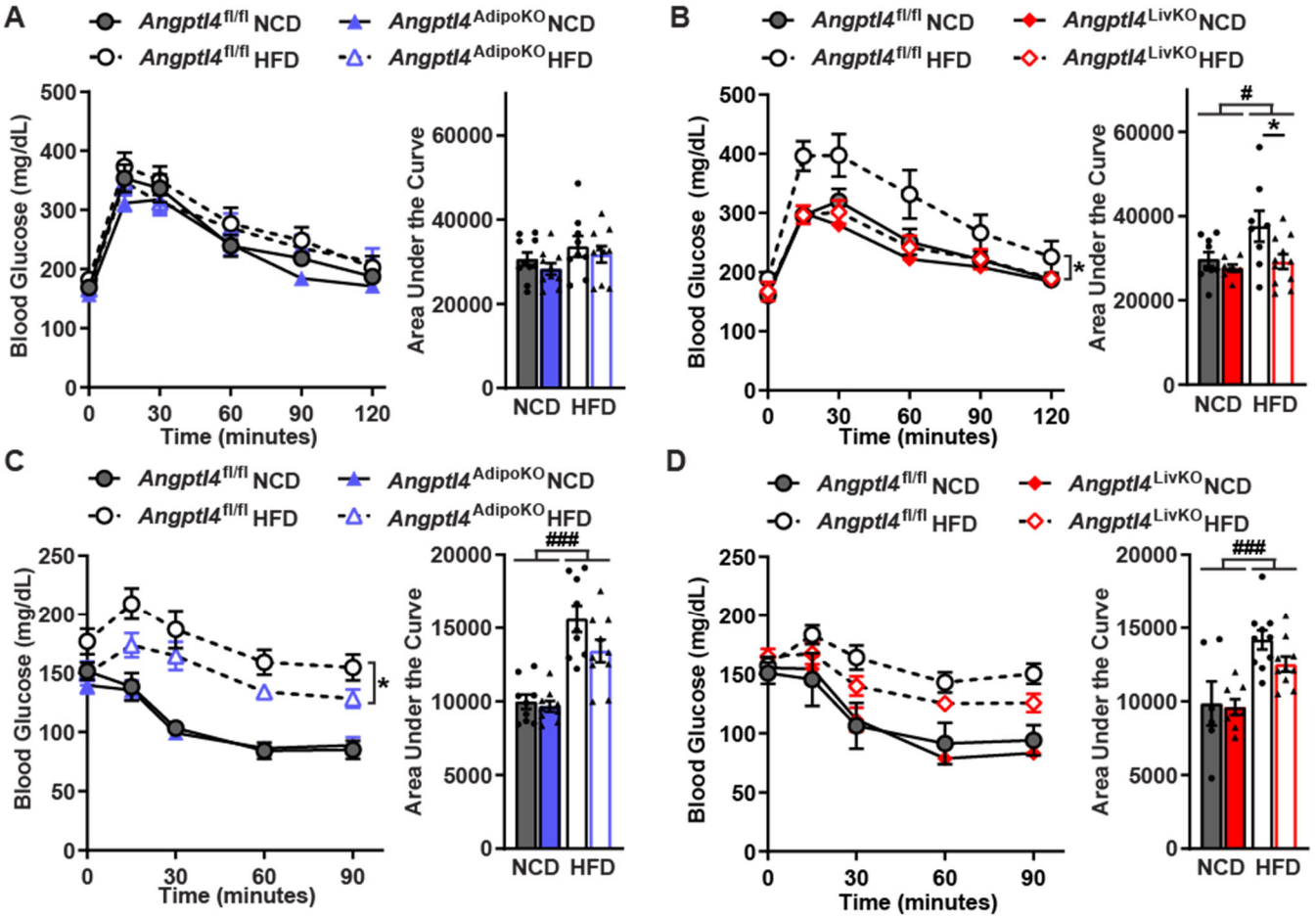

Figure 12. Glucose tolerance and insulin sensitivity of *Angptl4*^{AdipoKO} and *Angptl4*^{LivKO} mice after chronic high fat feeding. A and B) Glucose tolerance tests were performed on fasted (6 h) male *Angptl4*^{AdipoKO} (A) and *Angptl4*^{LivKO} (B) mice after 24 weeks of either a normal chow diet (NCD) or high fat diet (HFD). Mice were injected with glucose (1 g/kg) and blood glucose concentrations were measured over 2 hours. Points represent glucose levels (mean±SEM; n=6-10) at each respective time point. Bar graphs represent area under the curve (mean±SEM) for all time points. *p<0.05 by repeated measures ANOVA. **C and D**) Insulin tolerance tests were performed on fasted (4 h) male *Angptl4*^{AdipoKO} (C) and *Angptl4*^{LivKO} (D) mice after 25 weeks of either a normal chow diet (NCD) or high fat diet (HFD). Mice were injected with 0.75 U/ml of human insulin (Humalin-R) and blood glucose concentrations were measured over 90 min. Points represent glucose levels (mean±SEM; n=5-9) at each respective time point. Bar graphs represent area under the curve (mean±SEM) for all time points. #p<0.05, ###p<0.001 for dietary differences by two-way ANOVA. *p<0.05, for individual genotype-specific differences by multiple comparison after two-way ANOVA (Tukey correction).